Peter Gluschitz, BSc

Analysis of the thermal degradation of commercial 18650 and pouch lithium-ion cells

Masterarbeit

zur Erlangung des akademischen Grades eines

Diplom-Ingenieur

Verfahrenstechnik

eingereicht an der

Technischen Universität Graz

Betreuer:

Assoc.Prof. Dipl.-Ing. Dr.techn. Hacker, Viktor

Dipl.-Ing. Lammer, Michael

Institut für Chemische Verfahrenstechnik und Umwelttechnik

Graz, Oktober 2017

EIDESSTATTLICHE ERKLÄRUNG

Ich erkläre an Eides statt, dass ich die vorliegende Arbeit selbstständig verfasst, andere als die angegebenen Quellen/Hilfsmittel nicht benutzt, und die den benutzten Quellen wörtlich und inhaltlich entnommenen Stellen als solche kenntlich gemacht habe. Das in TUGRAZonline hochgeladene Textdokument ist mit der vorliegenden Masterarbeit/Diplomarbeit identisch.

STATUTORY DECLARATION

I declare that I have authored this thesis independently, that I have not used other than the declared sources / resources, and that I have explicitly marked all material which has been quoted either literally or by content from the used sources. The text document uploaded in TUGRAZonline is identical to the present master thesis.

Graz, …… ……

(Datum / date) (Unterschrift / signature)

AUFGABENSTELLUNG

Li-Ionen-Akkumulatoren werden in elektronischen Geräten wie Smartphones und Notebooks aber auch in Fahrzeugen eingesetzt. Die Li-Ionen-Akkus weisen bei hoher Energiedichte eine gute Zyklenfestigkeit bzw. Alterungsbeständigkeit auf. Kritische Betriebszustände können jedoch zum thermischen Durchgehen führen, wobei es zu starker Hitzeentwicklung und zur Gasfreisetzung kommt. Im Projekt ISALIB wird das intrinsische Risiko des thermischen Durchgehens abhängig von verbauten Materialien (Anodentyp, Kathodentyp, Elektrolyt) und der Fehlerart (Übertemperatur, Überladung usw.) untersucht. Das Ergebnis ist eine umfassende Risikobewertung relevanten Li-Ionen-Batterietypen.

ASSIGNMENT

In electronic devices such as smartphones and notebooks, but also in vehicles, Li-ion battery systems are used. Li-ion accumulators have good cycle durability and aging resistance at high energy densities respectively. Critical operating conditions can lead to a thermal runaway, which is characterized by intense heat development and gas emissions. In the ISALIB project, the intrinsic risk of thermal runaway is investigated depending on the materials used (anodic, cathodic, electrolyte) and the type of fault (overtemperature, overloading, etc.). The result is a comprehensive risk assessment of relevant Li-ion battery types.

KURZFASSUNG

Der Lithium-Ionen-Akkumulator ist nach dem aktuellen Stand der Technik aufgrund der hohen Energiedichte, Zellspannung und Zyklenfestigkeit, auch bei kleinster Bauweise, das wohl wichtigste Speichermedium für elektrische Energie. In Anwendungen wie im Smartphone, Notebook oder auch in der Elektromobilität ist der Li-Ionen-Akku nicht mehr wegzudenken.

Im Rahmen dieser Arbeit wurden sechs unterschiedliche 18650 Li-Ionen-Akkus und Smartphone-Akkumulatoren der Unternehmen Apple, Samsung und LG untersucht. Die Akkus wurden in einem Rohrreaktor thermisch bis zum terminalen Schadensfall beansprucht. Es wurde das emittierte Gasvolumen gemessen und analysiert und die Temperaturverläufe und Zellspannung aufgezeichnet. Die bei diesem exothermen Prozess entstehenden Gase beinhalten vorwiegend H_2, CO, CO_2 und kurzkettige Kohlenwasserstoffe wie C_2H_2, C_2H_4 oder C_2H_6. Beim thermischen Durchgehen werden Temperaturen von 800°C erreicht und das ausströmende Gasvolumen beträgt ca. 6000 cm³.

ABSTRACT

According to the state of development, the lithium ion accumulator is, due to its high energy density, cell voltage and cyclic life-time, even in smallest construction, one of the most important storage media for electrical energy. In the fields of application such as smartphones, notebooks or electro mobility the lithium ion cell is no longer indispensable.

Within the scope of this work, six different 18650 battery cells and smartphone accumulators of the companies Apple, Samsung and LG were examined. For this purpose, all cells were thermally stressed in a tube reactor until terminal failure. The emitted gas volume was measured and analyzed and the temperature profiles and cell voltage were recorded. The gaseous emissions produced by this exothermic process mainly contain H_2, CO and CO_2 and short-chain hydrocarbons such as C_2H_2, C_2H_4 or C_2H_6. During the thermal runaway, temperatures of 800 °C are reached and the exhaust gas volume is about 6000 cm³.

CONTENT

1 INTRODUCTION

Too long we have been dependent on fossil fuels to heat our homes, to power our industries and for transportation. The present energy economy based on fossil fuels is facing serious issues. The burning of fossil fuels is accounted for emissions that contribute to global climate change, acid rain, and ozone problems [2].

At one hand our society becomes more dependent on hi-tech equipment, which need high electrical energy but on the other hand climate change issues by CO_2-emissions, and its effects on nature and humanity are coming more and more into the focus. The consequences of constantly increasing greenhouse gas emissions in the atmosphere such as rising temperature and sea levels, acidification of the oceans, extended droughts as well as more frequent flooding can be attributed to the anthropogenic burning of fossil fuels [3]. In order to keep the impact of climate change moderate, new ways of energy production and utilization must be found. For that reason scientists and companies around the world are looking for alternative ways to produce and store the energy of renewable resources. These technologies have to overcome the various advantages of fossil fuels while competing with their relatively low price. The advantages of fossil fuels are mainly their widespread availability, well established infrastructure, high energy density and good transportability. Most renewables such as wind, hydro and solar power have the disadvantage of not being available continuously and everywhere. Therefore one of the main bottle necks for the development of a sustainable energy system is the storage of electricity from alternative, delocalized sources [4]. One of the key energy devices as capable energy system is the lithium ion battery (LIB).

The lithium ion battery has a high power density, long life cycle and low self-discharge properties. Therefore, LIB applications have a wide attention, from very small cells in smartphones to large devices in electrical vehicles. But the thermal instability of LIB must also be considered. Among the various LIB, those with a lithium cobalt oxide (Li_xCoO_2) cathode has been commonly used as a power source for portable electronics, and lithium manganese oxide ($Li_xMn_2O_4$) batteries have been used for electronic hand tools because of their capacitance and safety properties [5]. There are more lithium oxide compounds, which are not describe in this work. The chemistry, performance, cost and safety characteristics vary among the different commercial LIB types, which have been common in consumer electronics. The LIB is one of the

most popular battery types for portable electronics, such as cellular phones, portable PCs and others (more than 90% of battery packs use Li-ion cells), and they have one of the best energy-to-weight ratios, no memory effect and a slow loss of charge when not in use [6].

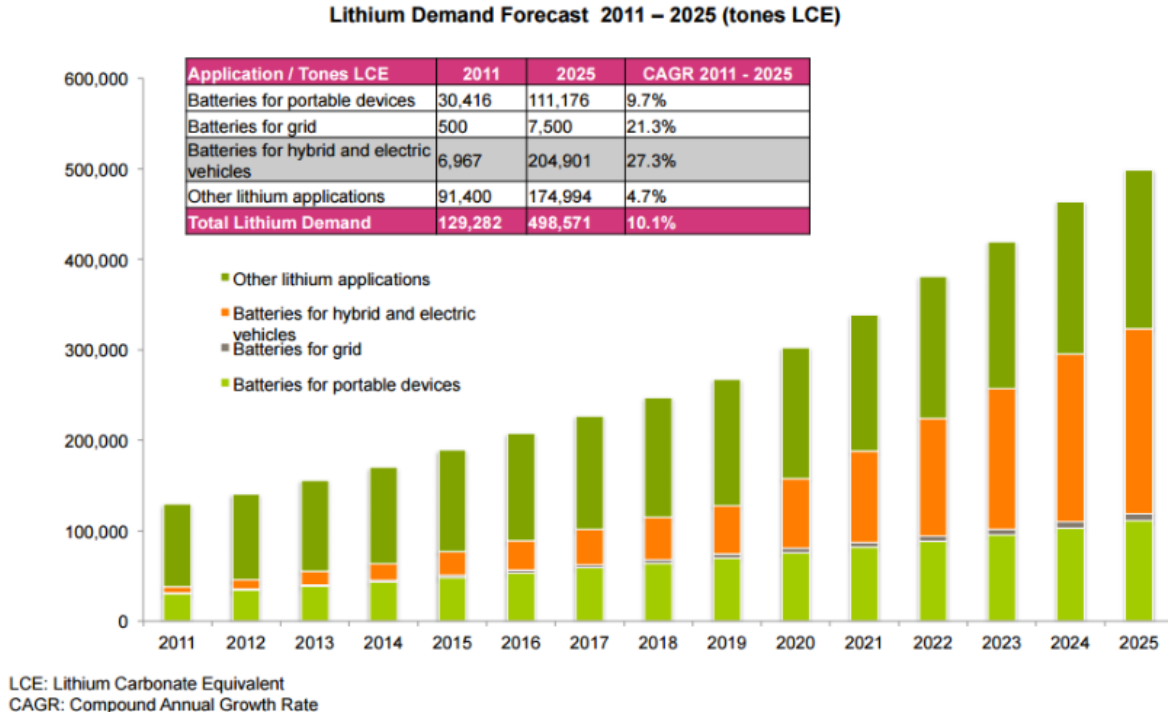

Figure 1: Worldwide development of the requirement of Li-ion batteries in devices per year [7].

Figure 1 gives an overview of the impressive development of the Li-ion market.
With a constant increase in capacity and the start of mass production by different competitors the prices have dropped significantly while the production amount grew annually. LIB have several advantages over conventional nickel metal hydride (NiMH), nickel cadmium (NiCd) or lead acid batteries, making them the technology of choice especially for portable applications where high energy density is needed. They have a higher nominal voltage due to their anode and cathode materials, higher capacity and energy density as well as almost no memory effect and a longer shelf life. They can be charged and discharged quickly with rates several times their capacity. For usage as power supply for automotive applications high energy and power is needed to maximize range and acceleration.

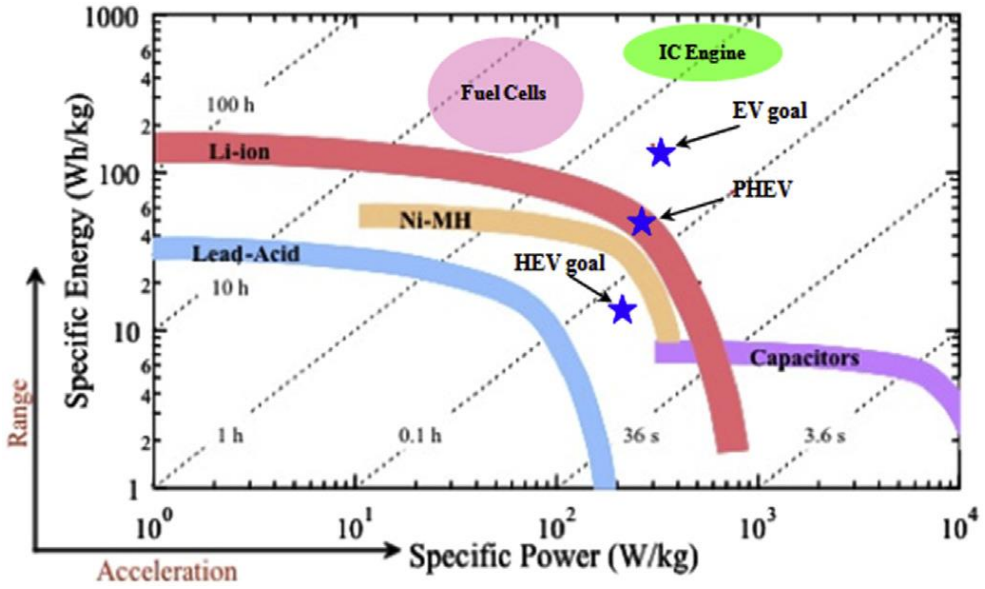

Figure 2: Ragone plot of energy storage device for automotive applications [6].

Figure 2 gives an overview of the specific energy and power of several energy systems for automotive applications (hybrid electric vehicles (HEV), plug in hybrid electric vehicles (PHEV) and electric vehicles (EV)). The specific energy of batteries (the capacity for storing energy per kilogram of mass) is still only around 2% of the specific energy of gasoline. Unless there is a major breakthrough, batteries will continue to limit the driving range of electric vehicles to 300 kilometers between charges [4,8]. Specific power is especially important in hybrid vehicles because they quickly charge/discharge large amounts of energy. It has to be the goal of the industry to strongly increase the nominal energy densities of the whole battery packs since the packs make up more than 25 percent of the mass of the whole car, thus limiting the range even more. It can be seen that the internal combustion (IC) engine still has the best characteristics regarding specific energy as well as specific power. But the efficiency of combustion engines is limited by Carnot's theorem. Because much heat is generated which can´t be used, their efficiency is only around 40 percent. The good energy result is mostly due to the high specific energies of the liquid fuels which are near to 13.000 Wh/kg [4,8,9].

Despite all features it must be noted that batteries contain both the fuel (negative electrode) as well as the oxidizer (positive electrode) emerged in an often flammable electrolyte and closely packed in a sealed containment. With this construction risks for direct reactions between fuel and oxidizer can occur. During normal operating

conditions LIB electrochemically convert this energy into electricity and can be regarded as relatively safe. Nevertheless there have been some serious incidents and accidents related to the self-heating of Li-ion batteries. In 2006 Sony had to recall almost as many as 6 million Li-ion laptop batteries after numerous reports of spontaneous self-igniting accumulators used in Apple and Dell notebooks [10]. Several fire accidents have been reported onboard cargo and passenger airplanes which can be traced back to the overheating of batteries [11]. There are serious safety concerns especially under abusive conditions such as increased temperatures, short circuits, mechanical damage, overcharge or underdischarge. Under these exceptional conditions the cells can develop a significant amount of heat which in the worst case can lead to a catastrophic, exothermic process called thermal runaway (TR). Thermal runaway is an event where the cell materials react directly inside the cell, which leads to an undesirable amount of heat generated by the cell. Thermal runaway can be triggered by abusive conditions and can happen spontaneously [12].

1.1 Basic concepts of the lithium ion battery

Li-ion batteries are mostly produced as prismatic, cylindrical or pouch cells with metals or polymers used as housing material. A clear distinction is made between Li-ion batteries and lithium polymer batteries. The main difference between them is the electrolyte which is in a liquid (Li-ion) or in a polymer state (Li-polymer). This work solely investigates cylindrical Li-ion cells in the 18650 format and prismatic pouch Li-ion cells from Apple, Samsung and LG.

The three primary functional components of a lithium ion battery are the anode, cathode, and electrolyte.

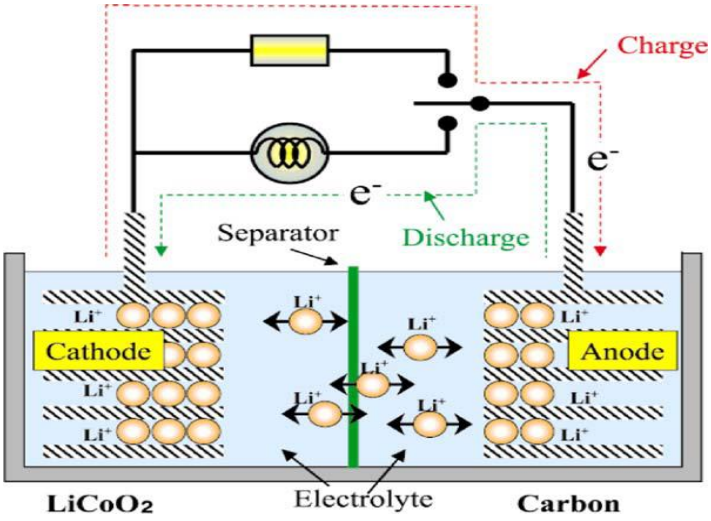

Figure 3: Schematic of the principle of LIB [11].

The anode of a conventional lithium ion cell is made from carbon, the cathode is a metal oxide and the electrolyte is a lithium salt in an organic solvent. The commercially most popular anode material is graphite. The cathode is generally one of three materials: a layered oxide (such as lithium cobalt oxide), a polyanion (such as lithium iron phosphate), or a spinel (such as lithium manganese oxide). The electrolyte is typically a mixture of organic carbonates such as ethylene carbonate (EC) and diethyl carbonate (DEC) containing dissolved lithium ions. These non-aqueous electrolytes generally use non-coordinating anion salts such as lithium hexafluorophosphate ($LiPF_6$), lithium hexafluoroarsenate monohydrate ($LiAsF_6$), lithium perchlorate ($LiClO_4$), and lithium tetrafluoroborate ($LiBF_4$). A separator is necessary to separate the anode and cathode. The separator is a very thin sheet of micro-perforated plastic. It is located between the cathode and the anode and separates the positive and negative electrodes while allowing ions to pass through. When a lithium ion battery is charged, lithium ions move from its cathode to its anode, while electrons flow in through an external electrical circuit. The process is reversed during charge/discharge, as shown in Figure 3 [13]. The more lithium the electrodes can take in, the more total energy the battery can store. Most types of batteries are based on the $LiMn_2O_2$ or $LiCoO_2$ sequence and operate on a process [14]:

The cathode half-reaction for $LiMn_2O_2$ is:

$$\boldsymbol{LiMn_2O_2} \underset{\boldsymbol{discharge}}{\overset{\boldsymbol{charge}}{\rightleftharpoons}} \boldsymbol{Li_{1-x}Mn_2O_2 + xLi^+ + xe^-} \qquad \textbf{(Eq. 1)}$$

The anode half-reaction is:

$$\boldsymbol{nC + xLi^+ + xe^-} \underset{\boldsymbol{discharge}}{\overset{\boldsymbol{charge}}{\rightleftharpoons}} \boldsymbol{Li_xC_n} \qquad \textbf{(Eq. 2)}$$

Full cell reaction is:

$$\boldsymbol{LiMn_2O_2 + nC} \underset{\boldsymbol{discharge}}{\overset{\boldsymbol{charge}}{\rightleftharpoons}} \boldsymbol{Li_{1-x}Mn_2O_2 + Li_xC_n} \qquad \textbf{(Eq. 3)}$$

Cathode materials may be $LiCoO_2$, $LiNiO_2$, $LiMn_2O_4$, $LiFeO_2$, $LiWO_2$. The anode materials may be $LixC_6$, TiS_2, WO_3, NbS_2, V_2O_5, etc. [11].

1.2 Thermal runaway mechanism

Thermal runaway is one of the failure modes of batteries. Intense research has been conducted to find the exact cause of this issue [15]. Generally, thermal runaway occurs when an exothermic reaction goes out of control, that is the reaction rate increases due to an increase in temperature causing a further increase in temperature and hence a further increase in the reaction rate [16], which possibly results in an explosion. It is proposed that above 80 °C, thermal runaway can occur spontaneously as a result of fire or explosion or external heating [17]. For the lithium ion battery runaway, it is caused by the exothermic reactions between the electrolyte, anode and cathode, with the temperature and pressure increasing in the battery.

The temperature of a lithium ion cell is determined by the heat balance between the amount of heat generated and that dissipated by the cell [18, 19]. The heat generation follows the exponential function and the heat dissipation keeps the linear function [20]. When a cell is heated above a certain temperature (usually above 115–150 °C) [21, 22, 23], exothermic chemical reactions between the electrodes and electrolyte set in will raise its internal temperature. If the cell can dissipate this heat, its temperature will not rise abnormally. However, if the generated heat is more than what can be dissipated, the exothermic processes would proceed under adiabatic-like conditions and the cell's temperature will increase rapidly. The rising temperature will further accelerate the chemical reactions, rather than the desired galvanic reactions, causing even more heat to be produced, eventually resulting in thermal runaway [21].

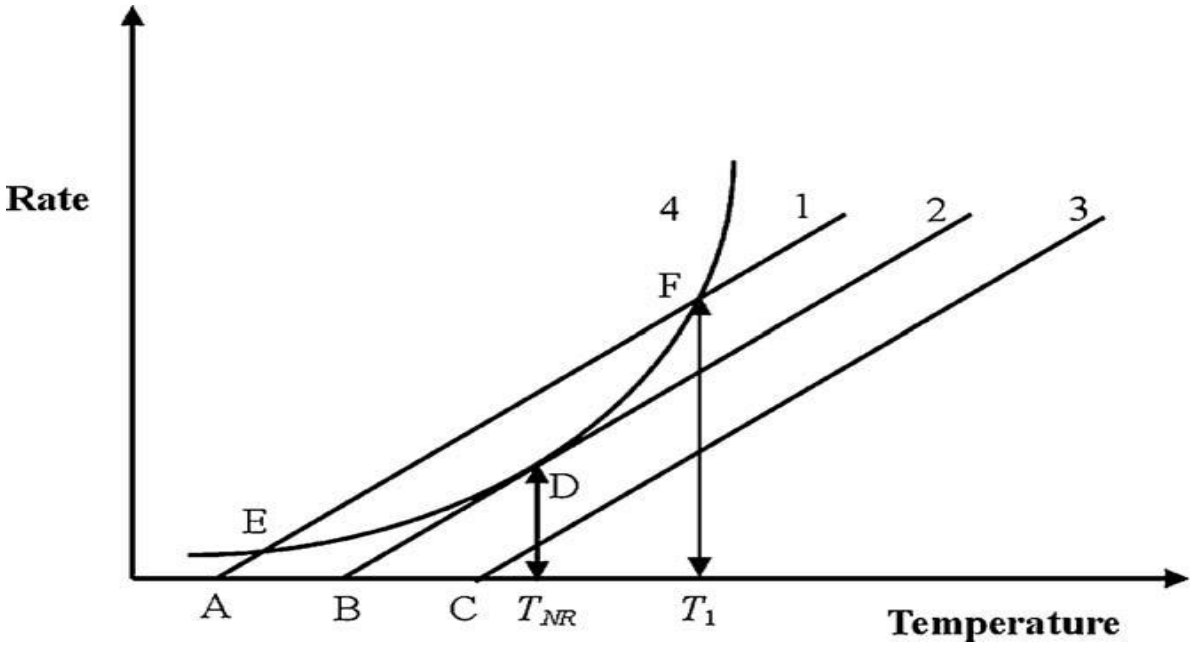

Figure 4: Semenov plot of a reaction and heat loss from a vessel, at 3 ambient temperatures, A, B, and C. A can control the sample to temperature T1, B is at the critical temperature TNR and C cannot control the thermal runaway. Adopted from Ref. [20].

An elegant way to visualize thermal runway reactions is in the plots often referred to as Semenov plots [24] in Figure 4. The curved line 4 represents the heat generation due to an exothermic reaction (exponential function, assuming Arrhenius law) while the straight lines represent the heat removal which is a linear function at different coolant temperatures. For the lithium ion battery, the curve 4 is the combined results of reactions occurred in the cell during the thermal runaway process. The temperature of the coolant can be sufficiently low (case of line 1) or insufficiently, like in case 3 where thermal control is not possible under any circumstances. Line 1 has two

points of intersection with line 4. Isothermal operation is possible in both points. The lower point E of intersection is a stable point. If temperature deviates upwards cooling power is higher than power generated by the reaction thus the system will return to the temperature of the stable point of operation. If temperature drops, as power generation is higher than power removal temperature will again return to that point. The second section (higher point F) is an unstable one. If temperature drops it will go on dropping until it reaches the stable point. But as energy removal is higher than energy generation and gets upwards the runaway is unpreventable. Line 2 has one tangent point D with line 4, this point is a critical point, as heat removal is equal to heat generation, and thus, this critical equilibrium temperature is called the 'Temperature of No Return' (TNR). The temperature B is called the self-accelerating decomposition temperature (SADT) [22]. The LIB can be regarded as a reaction system, in which heat is generated by the reactions between its compounds. Then, under different working and boundary conditions, when the battery temperature reaches the TNR, the thermal runaway will occur. The above Semenov plots can explain the thermal runaway process simply and clearly, in which the heat generated by the reactions is the key issue as it dominates the thermal runaway process [11].

The aim of this work is to identify and characterize the risks of 18650 format and Samsung, Apple and LG pouch cells. Especially the critical temperatures which trigger a self-accelerating thermal runaway event (T_{NR}), gas emissions and voltage during the whole process were investigated. Therefore different cell models of various manufacturers were tested under defined testing conditions. The results should help to provide fundamental data for better understanding the main failure modes in order to allow for the safe use and application of LIB [4].

2 EXPERIMENTAL METHOD

2.1 Investigated cells

The models, which were used in the experiments, were either new or cyclically and calendrically aged Li-ion cells of the 18650 format and commercially purchased new pouch cells from Apple, Samsung and LG. Cyclic aging of cells was achieved by the continuous charging and discharging of the cell, while calendrically aged cells were prepared by storing cells at 60 °C until reaching the stop criterion. For testing all cells were charged to the desired state of charge (SOC) of 100% by using a Battery Test System (BaSyTec, Type CTS-LAB, Basytec GmbH).

In three overcharge tests, triggering thermal runaway was attempted. To achieve a reproducible test environment all samples were carried out in the tube reactor. The charging cables from the BASYTEC were extended and placed inside the reactor. At the first attempt, the current was kept constant at 2 A while the voltage was set variable. The second was also charged with 2 A but with a defined high voltage of 12.6 V. In the last overcharge test, the voltage was kept at 12.6 V while the current was variably adjusted by the Basytec in response to the state of charge. In the following figure (Figure 5) the three different overcharge tests are displayed.

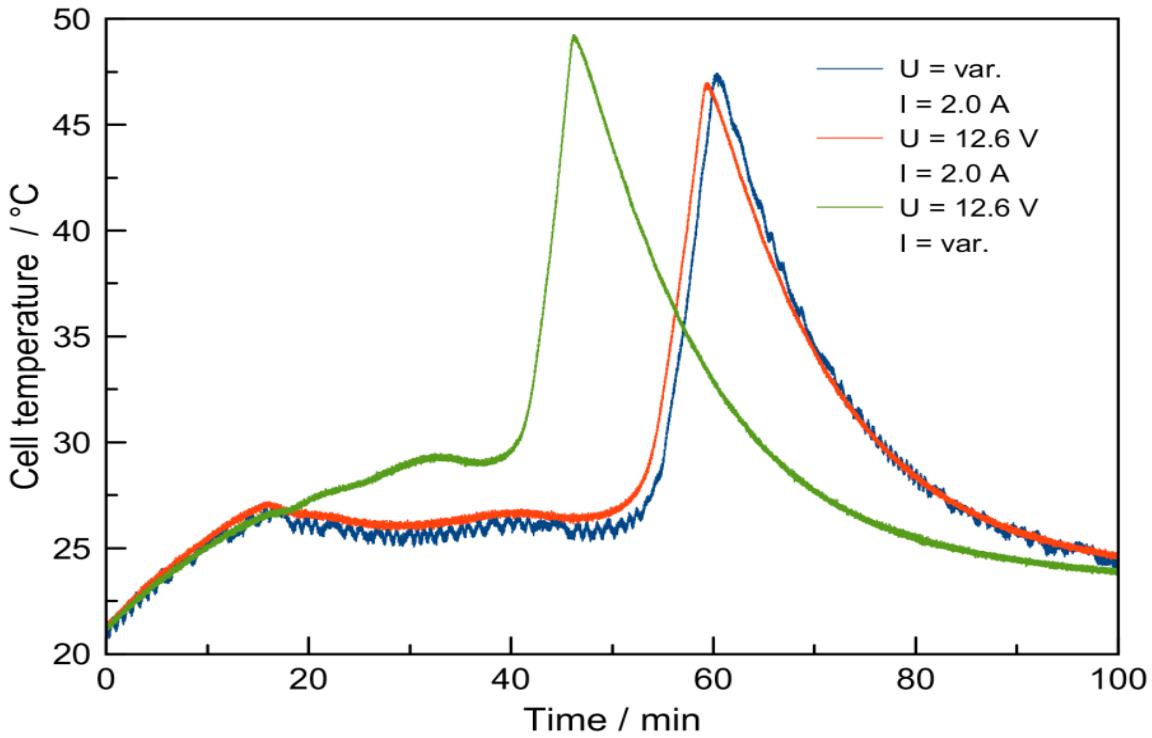

Figure 5: Temperature-time plot of the performed overcharge tests.

All other batteries where charged using a constant current/constant voltage (CC/CV) mode where the current is kept constant until the battery voltage is approaching the maximum charging voltage. When this voltage is reached, it is kept constant and the current is reduced until it falls below the minimum charging current of 50 mA. In this way, a complete and safe charging of the cells was guaranteed. After charging, the shrinkage foil from the 18650 cells was removed from the battery shell and the bare steel cells were weighed before being mounted inside the test reactor. The basic information of the tested cells is summarized in Table 1.

Table 1: Basic information about the tested cells, according to the manufacturer data sheet.

Cell type	Nominal capacity [mAh]	Cathode material	Cell mass * [g]
Samsung S6	2550	$LiCoO_2$**	33,19
iPhone 6S	1750	$LiCoO_2$**	25,19
LG 3G	3000	$LiCoO_2$**	46,19
NCR18650B	3350	$Li(NiCoAl)O_2$	45,29
NCR18650GA	3300	$Li(NiCoAl)O_2$	46,84
INR18650-35E	3500	$Li(NiCoAl)O_2$	47,65
INR18650MJ1	3500	$Li(NiCoAl)O_2$	45,66
LG18650HE4	2500	$Li(NiMnCo)O_2$	45,53
US18650VTC5A	2500	$Li(NiMnCo)O_2$	47,39

* Average of the mass of all cells from this type
** No datasheet could be found for this cell, which would have given the exact information of the cathode material of the cell, but from the experiments it must be deviate that it is $LiCoO_2$, but it was not possible to determine the proportions of Ni or Mn.

To perfectly understand the reactions taking place inside the cell before and during thermal runaway it would be highly beneficial to know the exact composition and mass split of the various components and parts inside every single cell type. Battery manufacturers typically are very reluctant when it comes to providing detailed information about the composition of their products. Sophisticated analytical studies would be necessary in order to evaluate the exact composition and structure of every cell type. This is not the purpose of this work and was done to some extend in a previous project within the department [4, 25].

2.2 Setup of the Test rig

All of the experiments were performed inside a heated, tubular, stainless steel reactor located inside a fume hood (Figure 6).

Figure 6: Complete test rig under the fume hood, 1) inert gas inlet and manometer, 2) flange, 3) tube furnace, 4) water displacement apparatus, 5) gas exhaust valve, 6) 16 port gas sampling valve, 7) scale.

The tubular stainless steel test reactor consisted of a 12-hole DN-60 flange at the front, a tube with 60 mm outer diameter in the middle and an 8 mm tube at the back side (outlet). It had a length of 775 mm with a wall thickness of 3.5 mm, which was

given a total reactor volume of 1680 cm^3. The flange was fixed with four M10 * 50 mm screws. Between the flange discs a sealing disc (SIGRAFLEX HD Graphite, V20011Z31) ensured the gas tightness. In addition, a manometer (WIKAI, 1-5 bar) was fixed at the inlet side of the reactor to indicate a possible overpressure. Around the reactor has been an electrically operated tube oven (GERO RES-E230 / 3, 3 kVA). The heating of the furnace is done either by the GERO RES AC power supply (for fast pre-heating) or a DC power supply (TTi EX, 300 W) for a controlled slow heating rate. The power supply was adjusted to a voltage of 35.2 V and a current of 2.0 A, this was corresponded to a heating power of 70.4 W. In order to achieve an ideal heating of the cell, all cells were placed as centrally as possible in the reactor. For the piping of the exhaust gas tubes, mainly 8 mm but also 6 mm stainless steel pipes were fitted with pipe fittings in order to connect the reactor output to the analysis equipment. According to the design of the experiment, the gas flow lead from the reactor to the gas sampling valve, the gas volume measuring device (water displacement) or the exhaust with manually actuated ball valves, check valves and T-adapter (FITOK, 316 stainless steel). A septum at the inlet allowed sealing the reactor and inserting the cables for online measurements of temperature and voltage inside the reactor. All relevant parameters were controlled and recorded using a data controller (National Instruments Q 9178 with NI9472, NI9421, NI9221, NI9213 I / O modules). An in-house created LabVIEW (National Instruments) program was used as a controlling interface and provided an online visualization, which made the test process demonstrative. The LabVIEW program enabled the control of the inert gas flow, the gas sampling process, the pipe heating and displayed the data of all relevant temperatures, the gas flow, the time and the type of gas sampling, the cell voltage and the gas volume. Inert materials were selected based on the reaction potential of the cell components and the exhaust stream. After closing the reactor with the flange, the entire apparatus was purged with nitrogen to ensure a constant and reproducible, noncombustible, inert atmosphere within the overall test setup. The inert gas flow (N_2, 5.0 purity) was controlled with a mass flow controller (Bronkhorst, F-201CV-1KO, 0-1000 ml/min). For safety reasons, the complete test equipment was installed in a fume hood. The complete scheme of the test stand and its periphery is shown in Figure 7.

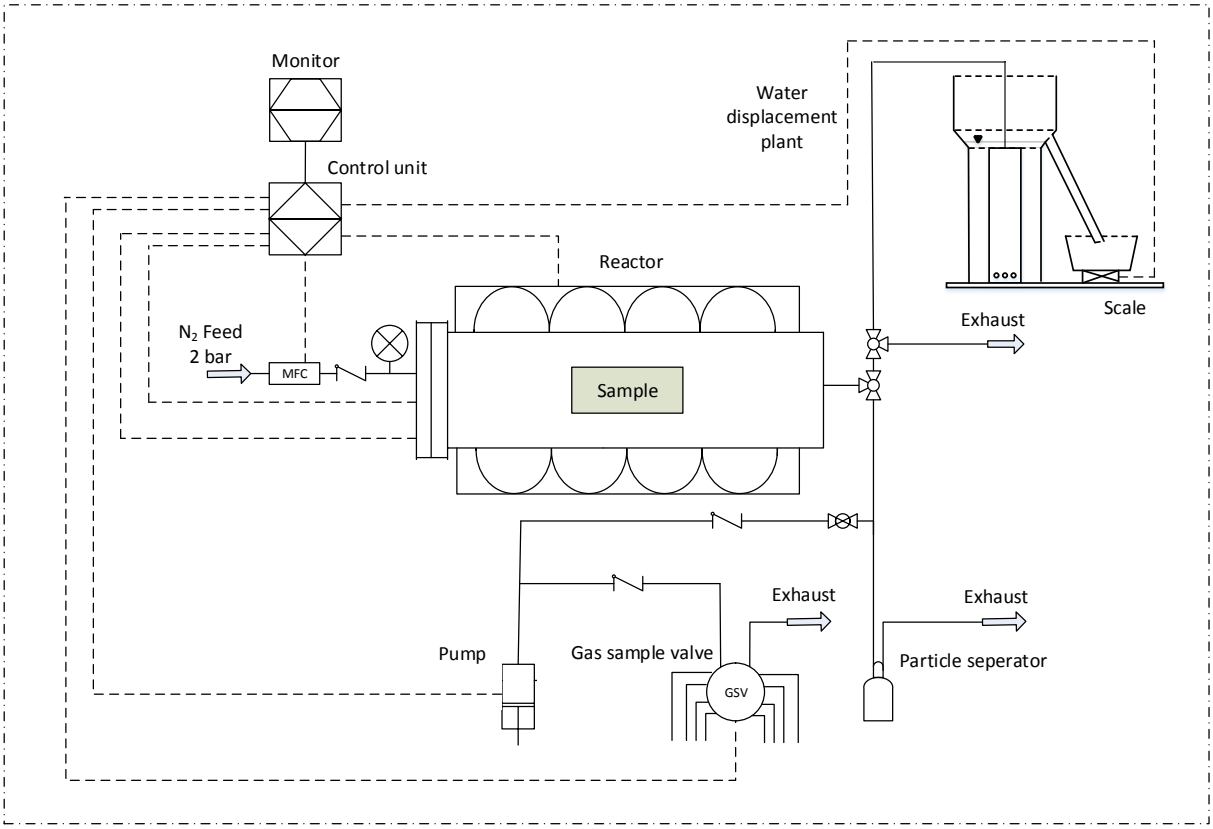

Figure 7: Piping and instrumentation diagram of the test rig and its periphery.

2.3 Test procedure

As a first step, the test cell was completely charged by using the BASYTEC. For the cylindrical 18650 cells the heat shrinkage foil was removed and the cell was weighed on a lab-scale (Kern 57-2, d=0.01g). After conditioning and weighing of the cell, three type K thermocouples were placed on the front, middle and end section of the cells in order to achieve high temporal resolution. The cell and the thermocouples were wrapped with Kapton tape (Figure 8 and 9). Two steel plates were installed in the sample holder to ensure the cell position within the sample holder. The upper part of the sample holder was also equipped with a K type thermocouple and adjusted to the lower part to close the sample holder.

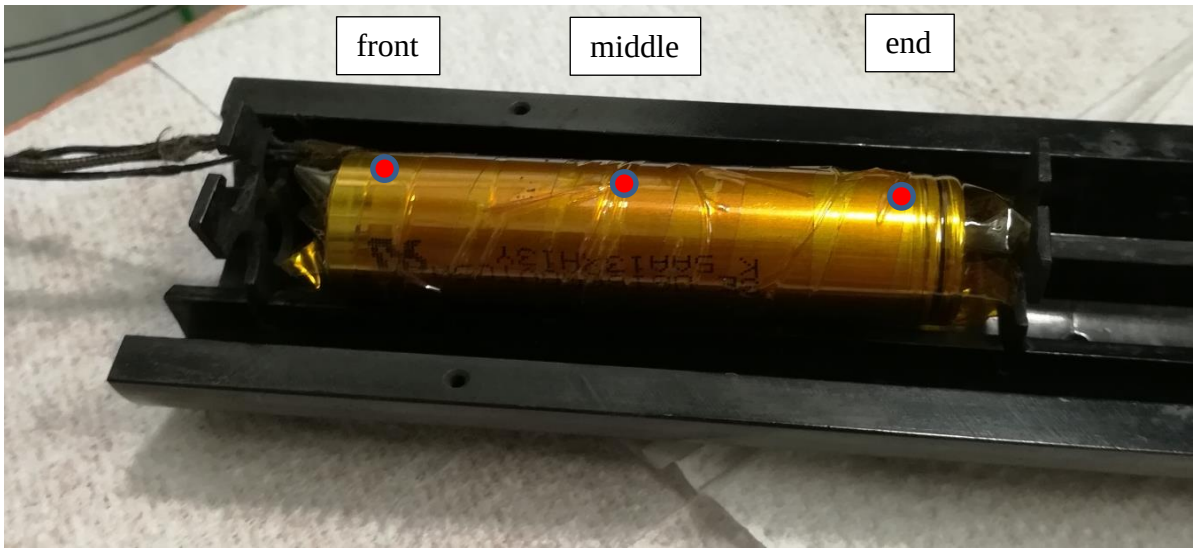

Figure 8: Stainless steel sample cell holder, containing an 18650 cell and thermocouples at front, middle and end of the cell (in the section of the red points).

As in the case of the 18650 cells, the K temperature sensors were attached at the front, the middle and at the end with Kapton tape (see Figure 8). Also was attached a temperature sensor on the upper side of the holder. The pouch cells were fixed in a special sample holder (Figure 9).

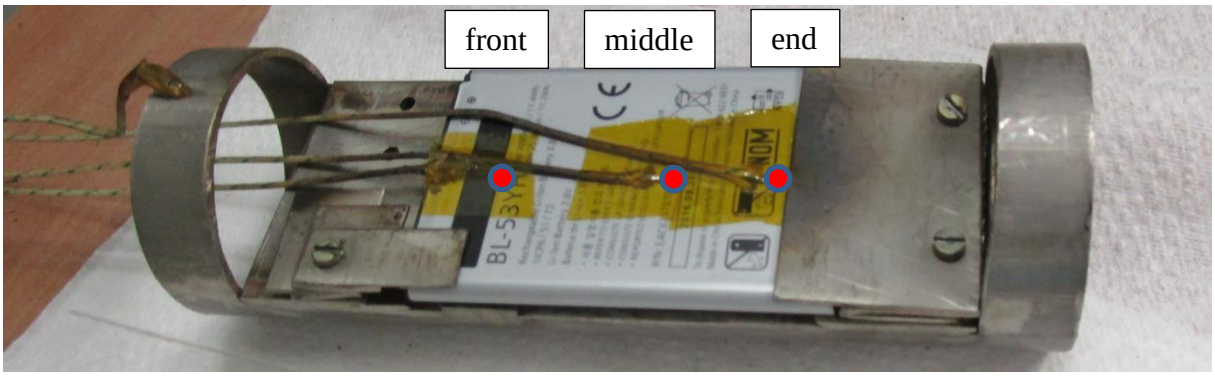

Figure 9: Stainless steel sample cell holder, containing an LG cell and thermocouples at front, middle and end (in the section of the red points).

Depending on the experiment, the sample holder for either 18650 or pouch cells was carefully inserted into the tube reactor. Steel bars were used as spacers to ensure that the sample holder was in the same location (in the center of the tube reactor) for each experiment. The reactor was then sealed with the flange and purged with nitrogen. After preheating the furnace to 80 °C with AC power, the heater was switched to DC power and the test was initiated with the start of the data acquisition. The reactor started to heat up with a defined heating rate according to the selected power con-

sumption (70 or 140 W). All experiments were carried out until to the thermal runaway. After this chemical process, the cells cooled again. The recording of data was turned off after the cells have cooled approximately to a temperature level similar to that of the furnace. After the entire system was cooled to room temperature, the reactor and sample holder were removed and cleaned with acetone. The residues of the cell were weighed to determine the mass change (Δm).

Either the released gas volume in connection with the current voltage was measured or gas samples were taken from the reactor exhaust gas via a bypass system. For this purpose, the reactor was continuously flushed with 70 ml/min of N_2 to transport the vent gas to the sampling valve.

In order to ensure a good comparison and a reproducibility of the experiments, three overcharge tests, five experiments each with the individual pouch cells and two with the individual 18650 cells were conducted (see also Table 1).

2.4 Gas chromatography and gas volume measurement

For qualitative and quantitative gas analysis of the gas samples a gas chromatograph was used (Agilent 3000A, Micro GC). The two-channel GC was equipped with two independent columns to detect a wide range of compounds. Channel A consists of a 5 Å molecular sieve column (320 µm diameter, 12 µm stationary phase thickness, 10 m length), which is heated to 110 °C with argon as carrier gas. The injection takes place in a backflush mode. Channel B was equipped with a PLOT U (320 µm diameter, 30 µm stationary phase thickness, 8 m length) column which was heated up to 80 °C and run in a fixed volume injection mode with helium as carrier gas. For one analysis run 0.5 cm³ of gaseous sample is drawn from the attached gas sample vial into the injector which is kept at 100 °C. The injector adds 0.01 cm³ samples onto the heated columns which are at 2.8 bar of carrier gas pressure. The running time for channel A was set to 70 s with a backflush time of 9.5 s while channel B had a running time of 60 s. [4] The method was adjusted and verified with commercially purchased analytical test gases. The exact specification of the used gases was summarized in Table 2.

Table 2: Specification of the gases used for chromatographic analysis.

Element	Description	Composition
Carrier gas channel A	Analytical argon gas	Purity: 99.999 % inlet pressure 5.5 bar
Carrier gas channel B	Analytical helium gas	Purity: 99.999 % inlet pressure 5.5 bar
Test gas 1	Air Liquide crystal mix 1	H2: 88 vol.% CH4: 0.3 vol.% CO2: 0.4 vol.% CO: 0.2 vol.% N2: rest
Test gas 2	Air Liquide crystal mix 2	H2: 72 vol.% CH4: 1.5 vol.% CO2: 3.0 vol.% CO: 2.5 vol.% N2: rest
Test gas 3	Air Liquide crystal mix 3	H2: 30 vol.% CH4: 15 vol.% CO2: 30 vol.% CO: 12 vol.% N2: rest
Test gas 4	Linde C2 calibration gas 1	C2H2: 1 vol.% C2H4: 1 vol.% C2H6: 1 vol.% N2: rest
Test gas 5	Linde C2 calibration gas 2	C2H2: 5 vol.% C2H4: 5 vol.% C2H6: 5 vol.% N2: rest

Over a bypass line an electrically controlled 16-port valve (SD16MWE-15D, Vici AG, Switzerland) was used to draw the samples. This 16-port valve allowed the in-situ sample collection of 8 gas samples at defined moments. The 8 gas vials (5 cm^3 glass vials) where sealed with a septum. The advantage of a 16-port valve by experiments with 8 samples is that after each sample could be switched into an empty exhaust gas channel, this ensured a consistent sampling. Before the experiments, all pipes and vials where flooded with inert gas (Ar, 5.0 purity). Due to the constant flow of inert gas (70 cm^3/min of N_2) through the reactor, the gas sample taken at a specific time corresponded to the generated gas of the cell at this moment. Immediately after the sampling, the vials were transferred to the gas chromatograph and three analytical runs were performed on each sample.

The gas samples were taken at the points of interest, which is explained below and shown in Figure 10. Figure 10 illustrates the moments at which the 8 gas samples were drawn from the reactor over a bypass system and transferred into the corresponding gas sample vials. The points of sampling where consistent for every experiment in order to allow the comparison of the different cell types. Samples were taken

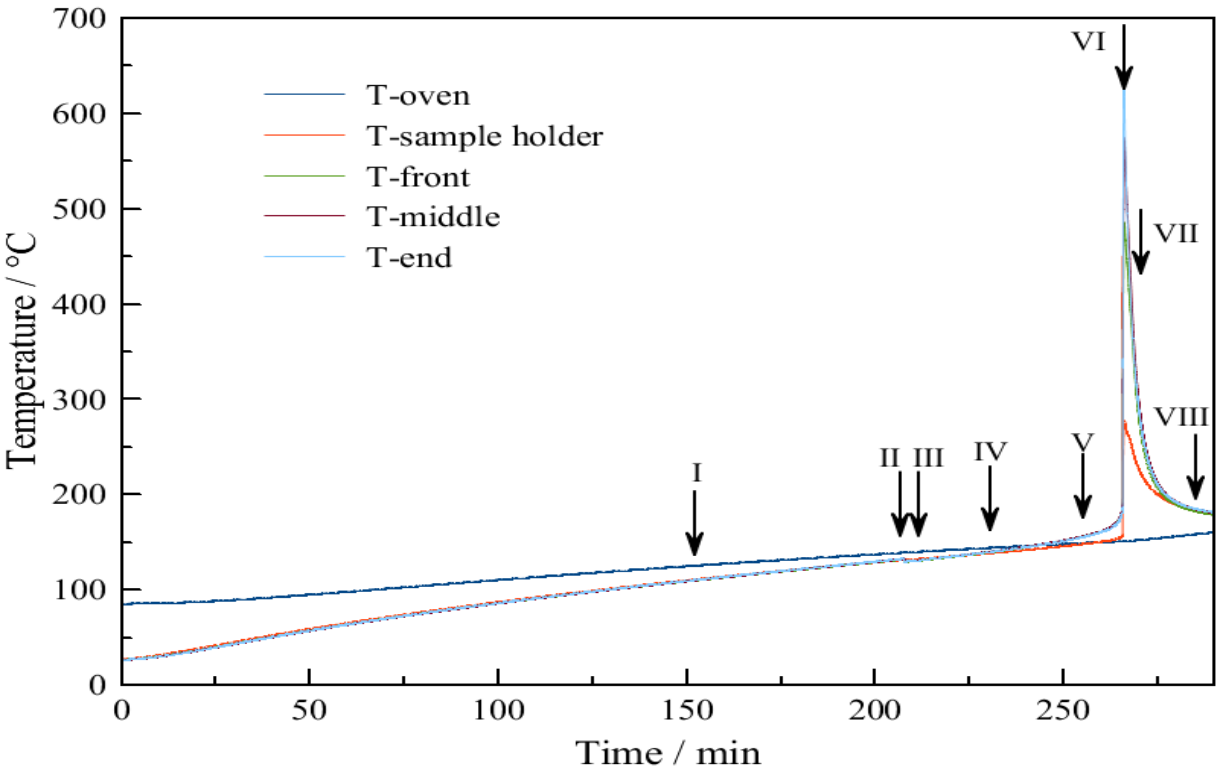

Figure 10: Temperature vs. time plot of a thermal ramp experiment, the points of sample taking for the gas analysis are indicated by roman numerals.

shortly before the 1st venting and the thermal runaway and after these events. These points were chosen and give information about the gas evolution from the cell. The gas samples were taken:

1. Before the 1st venting of the cell
2. Immediately after the 1st venting
3. Seconds after the 1st venting
4. Between the 1st venting and the thermal runaway
5. Immediately before the thermal runaway, in the exothermic phase
6. Immediately after the thermal runaway event
7. Seconds after the thermal runaway event
8. 20 minutes after the thermal runaway event

A water displacement apparatus measured the volume of the gas emission. The gas volume measurement was carried out independently of the gas analysis in a separate experiment in which no constant inert gas stream was applied. With the water displacement apparatus, the main processes, which led to gas generation, the first venting, the beginning of the exothermic phase and the thermal runaway, were determined in a time resolved manner.

The water displacement device is a custom made construction system consisting of two PVC pipes telescoped and fixed on a base plate. Holes on the underside of the inner tube closed both tubes together and defined the maximum gas volume to 10 000 cm³. The entire apparatus was filled with water and the inner tube was connected to the gas outlet of the reactor. When the pressure builds up inside the reactor due to gas evolution, it pushes the water level down inside the inner tube, resulting in an upward stroke of the water level in the outer tube. The basic concept of the device is shown in Figure 11. The displaced water from the outer pipe runs through an outlet on the scale (core PRS 12200, maximum 12 200 g, d = 0.1 g), which is connected to the data acquisition. The volume of the displaced water corresponds to the volume of gas evolution [4].

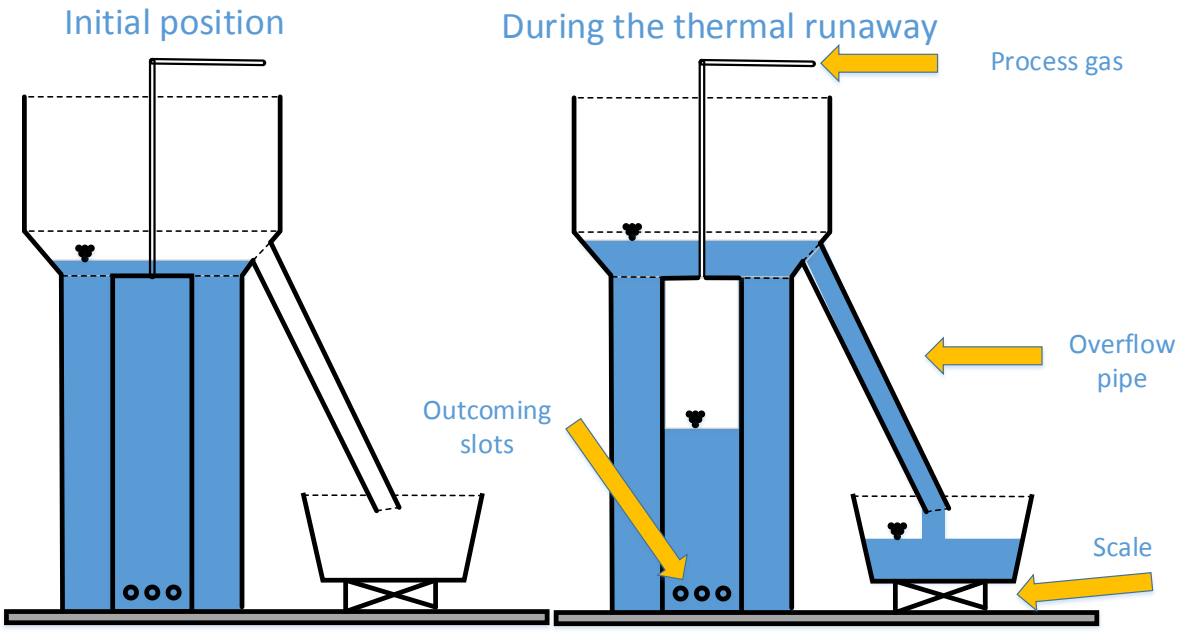

Figure 11: Scheme of the water displacement apparatus. The water level before the experiment (left) and the water level after gas evolution (right) were illustrated.

2.5 Data evaluation

Starting from the data sheets [26-31] of the individual 18650 cells, the initial conditions were used to investigate the thermal runaway and voltage process. Some experiments were performed using variations from the standard techniques to provide new insights and identify possible correlations. These variations are mentioned in the respective results. Many of the results are also related to the results of the work of A. Königseder [4].

2.6 Experimental data analysis

The gas volume and open cell voltage were simultaneously measured for each cell type. From these records, the measurement points for the individual gas samples were then determined. After the gas sample tests, all data were collected and compiled into plots for the interpretation of the experiments. Figure 12 shows the characteristics of the individual ramp tests. Points of interest are the first venting, which occurs at temperatures between 115 and 150 °C, the smooth transition from endothermic to exothermic phase and the end of the thermal runaway when the reactant was completely consumed.

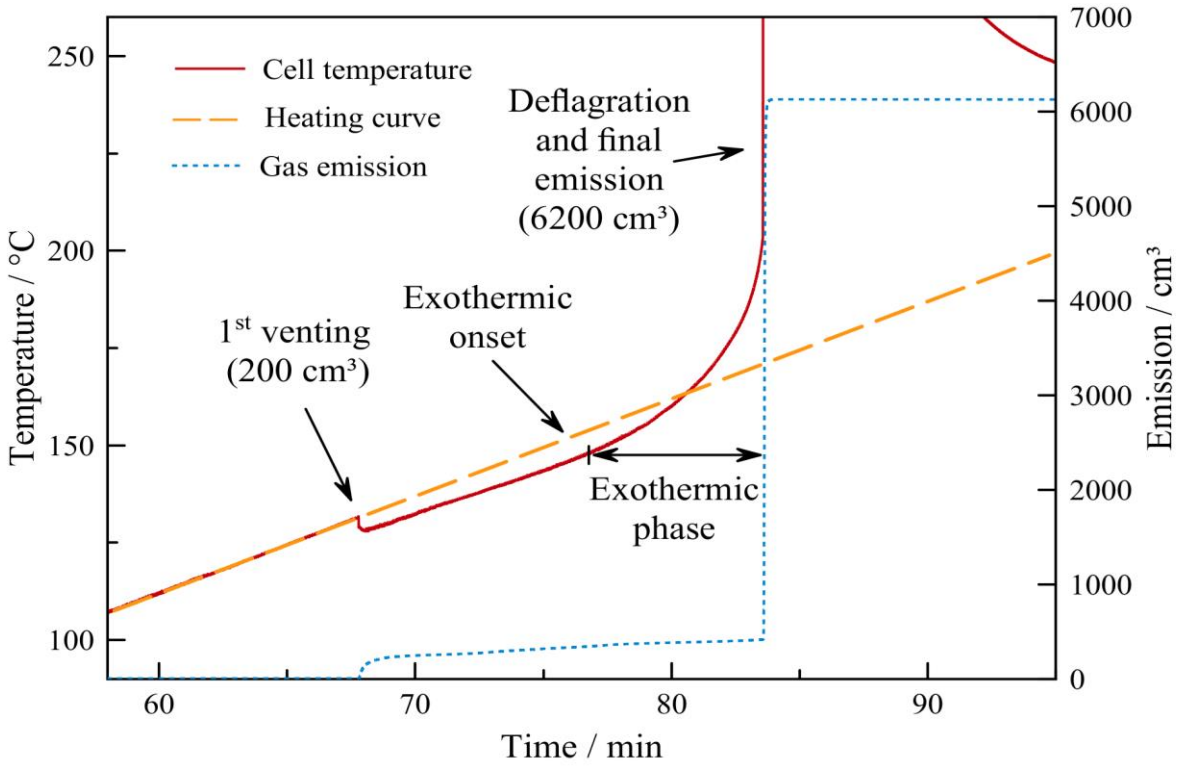

Figure 12: Accurate plot of the 1st venting, the exothermic onset until to the thermal runaway.

Figure 13 displays the stages of the individual phases of the experiments, the Heat up (stage 1), the accelerated heating (stage 2) and the thermal runaway (stage 3).

Heat up (stage 1): This first stage lasted from room temperature until it reached the exothermic onset temperature (T_{ONSET}). In this phase, the cell itself did not generate a significant amount of heat. The temperature increase was a result of the heating by the furnace. The first venting of the cell normally took place in this phase.

Accelerated heating (stage 2): T_{ONSET} marks the smooth transition from stage 1 to stage 2. In stage 2 the cell becomes a heat source due to the initial exothermic decomposition processes within the cell. These processes are strongly temperature-dependent and begin to accelerate exponentially with rising temperatures.

Thermal runaway (stage 3): This stage is the thermal runaway. It was starting with a heating rate of 2 °C/min for experiments with 70 W and 4 °C/min by 140 W furnace performance (T_{TR}). The thermal runaway took place in only a few seconds and was accompanied by a violent venting. The event was ended when all the reactants were consumed. In Figure 13 this is seen by reaching the maximum cell temperature (T_{max}) and the cooling process of the cell after the thermal runaway. [4, 12, 32]

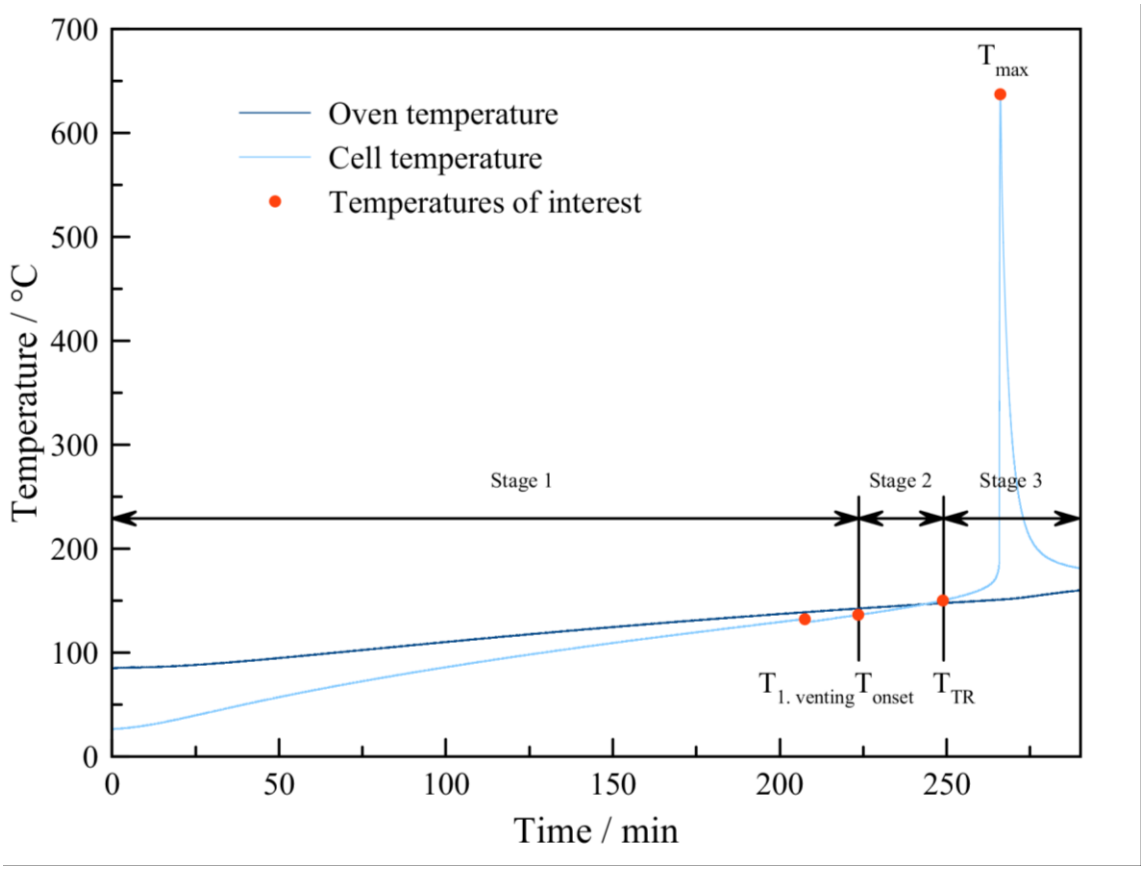

Figure 13: Classification of the stages – stage 1 lasting until the exothermic onset, stage 2 marking the accelerated heating and stage 3 the thermal runaway.

2.7 NCR18650B

The NCR18650B cell has a nominal capacity of 3350 mAh at a nominal voltage of 3.60 V. The average weight of the tested cells was 45.27 ± 0.06 g. The cell has a high capacity with a relatively low, continuous discharge current of 4.875 A. It is well suited for applications, which require a long run time at relatively low power consumption. The cathode material of this cell is $Li(Ni_{0.8}Co_{0.15}Al_{0.05})O_2$ and the anode consists of high density graphite. The experiments of the NCR18650B cell will be referred to as cell B and is shown in Table 3.

Table 3: Experiments of the B cell (VM = volume measurement, GC = gas chromatography, OCV = open circuit voltage).

Experiment	Type	Aging	Power [W]	Measurement
01	B	cycled	70	VM
02	B	cycled	70	GC
03	B	new	140	VM + OCV
04	B	new	140	GC

2.8 NCR18650GA

The NCR18650GA cell has a rated capacity of 3300 mAh at a nominal voltage of 3.60 V. The investigated cells had an average weight of 46.79 ± 0.12 g. The maximum, continuous discharge current, in combination with the high capacity, makes the cell a good choice for high power applications. The NCR18650GA cell will be referred to as GA cell. A list of all experiments with the GA cell is shown in Table 4.

Table 4: Experiments of the GA cell (VM = volume measurement, GC = gas chromatography, OCV = open circuit voltage).

Experiment	Type	Aging	Power [W]	Measurement
11	GA	cycled	70	VM
12	GA	cycled	70	GC
13	GA	new	140	VM
14	GA	new	140	GC + OCV

2.9 US18650VTC5A

The US18650VTC5A features a Li(NiMnCo)O2 cathode. The investigated cells had an averaged weight of 47.31 ± 0.22 g. The cells nominal voltage is 3.6 V and its nominal capacity is rated at 2500 mAh. The investigated VTC5A cells had offered the smallest capacities but the highest continuous discharge current of 30 A. Therefore it is particularly adapted for high power applications with short run-times. The US18650VTC5A cell will be referred to as VTC5A cell in this work. (List of all VTC5A experiments in

Table 5).

Table 5: Experiments of the VTC5A cell (VM = volume measurement, GC = gas chromatography, OCV = open circuit voltage).

Experiment	Type	Aging	Power [W]	Measurement
21	VTC5A	calendrical	70	VM
22	VTC5A	calendrical	70	GC
23	VTC5A	new	140	VM + OCV
24	VTC5A	new	140	GC

2.10 18650HE4

The 18650HE4 features a Li(NiMnCo)O_2 cathode and a nominal capacity of 2500 mAh and a nominal voltage of 3.60 V. The evaluated cells had an average weight of 45.50 ± 0.03 g. The low capacity and the very high continuous discharge current of 20 A make it a designated cell for high power applications. The 18650HE4 cell is referred as only HE4 cell. (All HE4 experiments see Table 6).

Table 6: Experiments of the HE4 cell (VM = volume measurement, GC = gas chromatography, OCV = open circuit voltage).

Experiment	Type	Aging	Power [W]	Measurement
31	HE4	calendrical	70	VM
32	HE4	calendrical	70	VM
33	HE4	new	140	VM + OCV
34	HE4	new	140	GC

2.11 INR18650-35E

The INR18650-35E cell is equipped with a $Li(Ni_{0.8}Co_{0.15}Al_{0.05})O_2$ cathode and has a nominal cell capacity of 3500 mAh and a nominal voltage of 3.60 V. The tested cells had a medium weight of 47.53 ± 0.10 g. With the high capacity and a high continuous discharge current of 8 A it is well suited for high power applications which also have high energy needs. The INR18650-35E cell is also referred as only 35E cell. All experiments of the 35E are shown in Table 7.

Table 7: Experiments of the 35E cell (VM = volume measurement, GC = gas chromatography, OCV = open circuit voltage).

Experiment	Type	Aging	Power [W]	Measurement
41	35E	cycled	70	VM
42	35E	cycled	70	GC
43	35E	calendrical	70	VM + OCV
44	35E	calendrical	70	GC + OCV
45	35E	new	140	VM + OCV
46	35E	new	140	GC

2.12 INR18650MJ1

The INR18650MJ1 cell has a nominal voltage of 3.64 V and a nominal capacity of 3500 mAh. The tested cells had an averaged weight of 45.93 ± 0.31 g. The high capacity in combination with the high continuously discharge current of 10 A makes the cell suitable for a wide range of high power and high energy applications. The INR18650MJ1 cell experiments are also referred as only MJ1 cell and are shown in Table 8.

Table 8: Experiments of the MJ1 cell (VM = volume measurement, GC = gas chromatography, OCV = open circuit voltage).

Experiment	Type	Aging	Power [W]	Measurement
51	MJ1	cycled	70	VM
52	MJ1	cycled	70	GC
53	MJ1	calendrical	70	VM + OCV
54	MJ1	calendrical	70	GC
55	MJ1	new	140	VM + OCV
56	MJ1	new	140	GC

2.13 Apple iPhone 6S

The smartphone iPhone 6S battery of the company Apple was bought in conventional trade. The battery was a very light, thin, pouch cell, which was layered built with the dimensions of 3.8x0.2x9.5 cm. The average weight of the tested cells was 25.52 ± 0.02 g. The LIB has a capacity of only 1715 mAh with a nominal discharge voltage of 3.82 V. The cathode material of this cell is $LiCoO_2$ and the anode consists of high density graphite. It is well suited for applications which require a long run time at relatively low power consumption. A list of all experiments with the iPhone battery is shown in Table 9.

Table 9: Experiments of the iPhone battery (VM = volume measurement, GC = gas chromatography, OCV = open circuit voltage).

Experiment	Type	Aging	Power [W]	Measurement
61	iPhone	new	70	VM
62	iPhone	new	70	GC + OCV
63	iPhone	new	70	GC + OCV
64	iPhone	new	70	GC + OCV
65	iPhone	new	70	VM + OCV

2.14 Samsung Galaxy S6

The smartphone Samsung Galaxy S6 battery was bought in conventional trade. The pouch cell with the dimensions of 4.1x0.3x9.2 cm was the biggest cell in this series. The average weight of the tested cells was 33.68 ± 0.03 g. The LIB has a capacity of 2550 mAh with a nominal voltage of 3.8 V. The cathode material of this cell is $LiCoO_2$ and the anode consists of high density graphite. It is well suited for applications which require a long run time at relatively low power consumption. The Samsung Galaxy S6 cell experiments are referred as SGS6 and were shown in Table 10.

Table 10: Experiments of the SGS6 battery (VM = volume measurement, GC = gas chromatography, OCV = open circuit voltage).

Experiment	Type	Aging	Power [W]	Measurement
71	SGS6	new	70	VM
72	SGS6	new	70	VM + OCV
73	SGS6	new	70	GC + OCV
74	SGS6	new	70	VM + OCV
75	SGS6	new	70	VM + OCV

2.15 LG G3

The smartphone battery from LG G3 was bought in conventional trade. The pouch cell with the dimensions of 5.1x7.4x0.5 cm was a powerful and affordable rechargeable smartphone battery of typical design. The short circuit, overvoltage and overheat protection was removed before each test. The average weight of the tested cells was 46.99 ± 0.01 g. The LIB has a capacity of 3000 mAh with a nominal voltage of 3.8 V. The cathode material of this cell is $LiCoO_2$ and the anode consists of high density graphite. In this work, the LG G3 cell is referred as LG. All experiments with LG battery are shown in Table 11.

Table 11: Experiments of the LG battery (VM = volume measurement, GC = gas chromatography, OCV = open circuit voltage).

Experiment	Type	Aging	Power [W]	Measurement
81	LG	new	70	VM
82	LG	new	70	GC
83	LG	new	70	GC
84	LG	new	70	VM + OCV
85	LG	new	70	GC + OCV

3 RESULTS AND DISCUSSION

The investigation of the thermal runaway, the gas emissions and open circuit voltage were conducted for six types of 18650 and 3 pouch smartphone lithium-ion battery cells.

3.1 Exemplary celltest: cycled B at 70 W oven performance

Figure 14 displays the temperature and gas emission profile over time of a cycled B cell heated using 70 W of power.

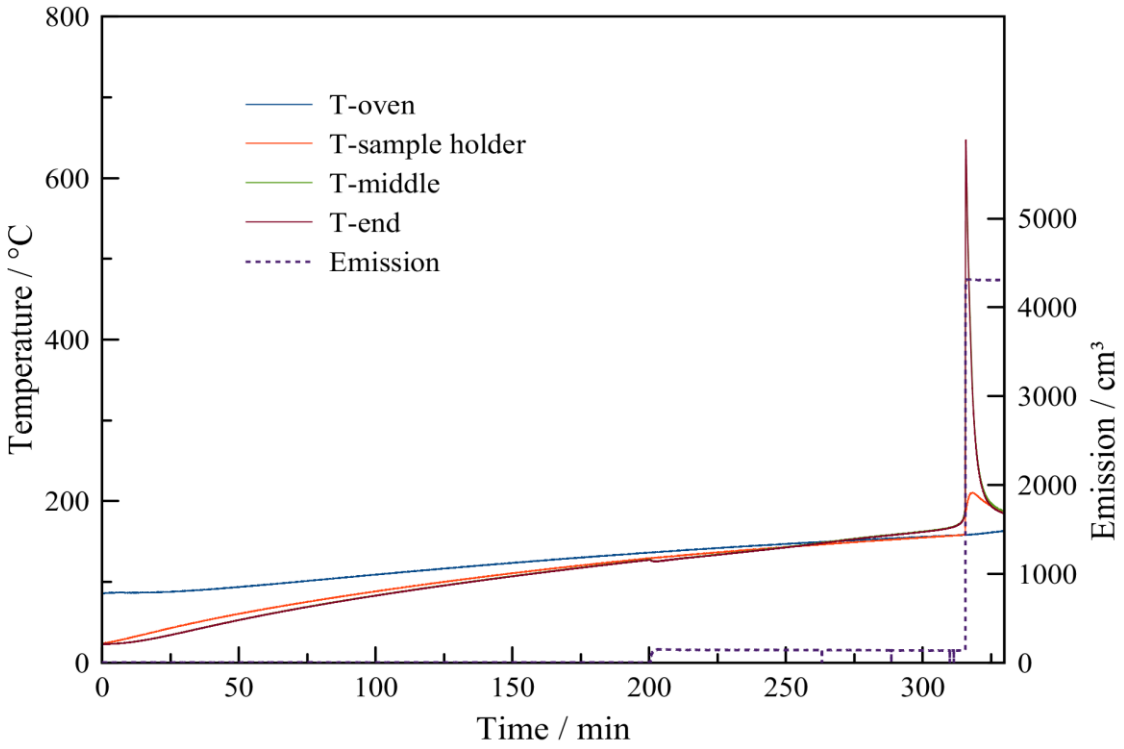

Figure 14: Temperature plot of a cycled NCR18650B cell (test: 01).

The furnace temperature at the beginning of the experiment was approximately 80 °C and increased constantly by the heating of the DC supply. The cell and the sample holder started at 24 °C and approached the oven temperature after 260 min. The thermocouple at the front of the cell was broken during the experiment and the corresponding curve was therefore removed from Figure 14. The cell vented at a cell temperature of 127 °C with a temperature drop of ≈ 4 °C. After the first venting, the cell temperature began to rise again with increasing rate. At a cell temperature of about

140 °C the cell temperatures exceeded the oven temperature, this indicated that the cell became a heat source. At a cell temperature of 169 °C the cell reached the thermal runaway onset temperature (starting at a rate of 2 °C/min, T_{TR}). The temperature climbed sharply, which also led to rapid heating of the sample holder.

Shortly after reaching T_{onset}, the cell went into a thermal runaway. A temperature of 647 °C (T_{max}) was reached. In combination with the 1st venting event and thermal runaway, an absolute gas volume of 4310 cm³ was generated during the experiment. Thereafter, the experiment was continued until the cell temperatures approached the temperature values of the furnace over a longer period of time.

3.2 Exemplary celltest: new B at 140 W oven performance

In these experiments commercially purchased B cells were used. 140 W of DC power were used for the heating of the cells. The above figure below (Figure 15) shows the temperature, emission and voltage over time.

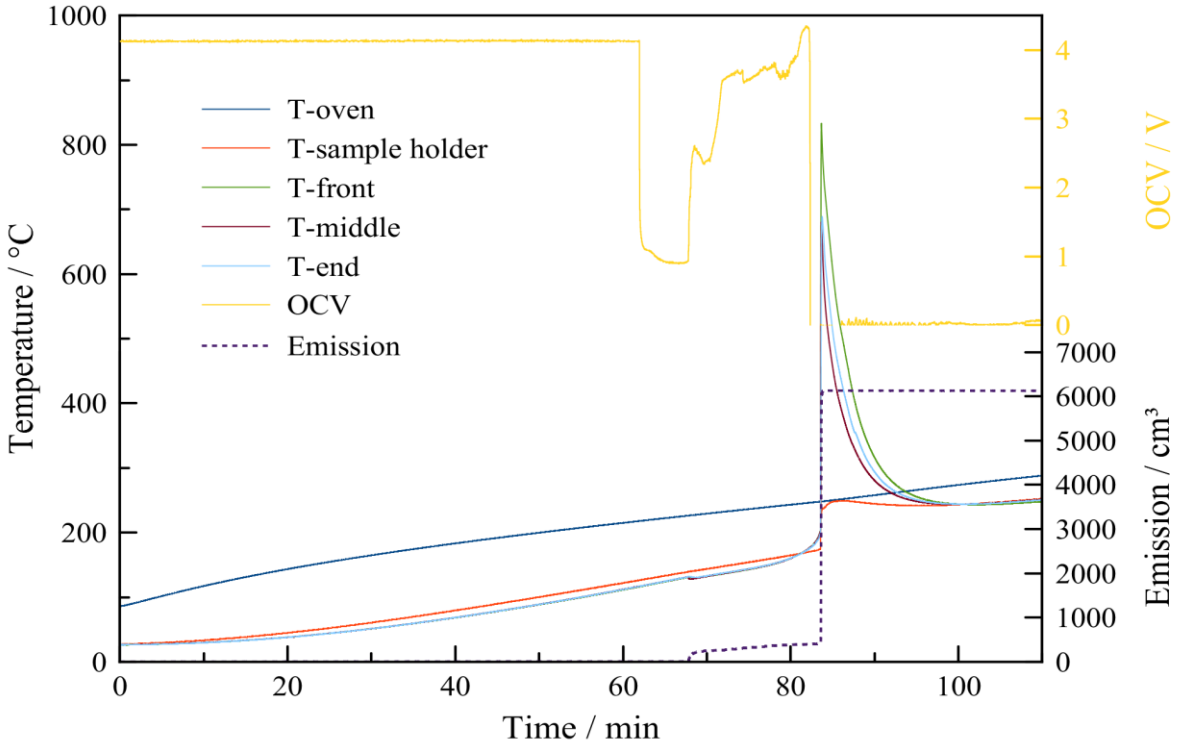

Figure 15: Temperature, emission and voltage plot of a new B cell by 140 W oven performance (test: 03).

The 140 W furnace performance resulted in a faster temperature rise of the cell and the sample holder. The oven temperature started at 80 °C and the cell and the sample holder at 24 °C. After only 68 min, the first outgassing of the cell took place at 131 °C with a temperature drop of ≈ 4 °C. Additionally the OCV (open circuit voltage) dropped. Shortly after the first venting, an abrupt temperature rise was observable, beginning at 151 °C by 4 °C/min. For this work, this rate was declared as T_{TR} for experiments with 140 W. Then the OCV rose slowly to its old level as the cell temperature rose with increasing rate.

At reaching T_{TR} the cell went into a thermal runaway and the OVC dropped irreversibly to 0 V. In this point a temperature of 688 °C (T_{max}) was reached. During the 1st venting event and thermal runaway an absolute gas volume of 6131 cm³ were produced throughout the experiment. Thereafter, the experiment was continued until the cell temperature approached the temperature values of the furnace over a longer period of time and no further changes were expected.

3.3 Analysis of B

Four experiments were carried out with the cell B. For this purpose, 2 new cells with a heating power of 140 W and 2 cells aged by cycling and an oven performance of 70 W were tested. For a better comparability the data was filtered for the points of interest only. The experimental results are summarized in Table 12.

Table 12: Summarized results of all experiments of B.

Experiment	m_{start} [g]	m_{end} [g]	Δm [g]	T_{vent} [°C]	T_{TR} [°C]	T_{max} [°C]	Emission [cm³]
01	45.33	17.26	28.07	127	169	647	4310.6
02	45.23	29.69	15.54	132	169	731	-
03	45.27	27.13	18.14	131	151	688	6131.1
04	45.32	23.86	21.46	137	150	796	-

As expected, the new cells with 140 W furnace performance reached the thermal runaway earlier and have got a slightly higher peak temperature with a larger emission of about 30% compared to the cyclically aged cells.

In addition to the heat and gas emission test, a separate experiment was performed to determine the composition of the gas that was developed during the thermal ramp test. During the heating phase of the cell only small amounts of gas were released from the reactor. This is mainly due to the expansion of the cumulative reactor volume, which is expanding with increasing temperatures. Immediately during the initial venting and thermal runaway of the cell, a significant gas evolution could be seen as a steep rise in the volume curve. (see Figure 14 and Figure 15)
Table 13 shows the gas composition of the cyclically aged and new cell immediately after the thermal runaway.

Table 13: Gas composition of the different B cells, each sample was taken immediately after the thermal runaway event.

Experiment	H_2 [%]	CH_4 [%]	CO [%]	CO_2 [%]	C_2H_4 [%]	C_2H_6 [%]	C_2H_2 [%]
02	22.07	4.51	57.80	14.26	1.06	0.10	0.20
04	76.32	18.14	0	0	4.40	0.66	0.48

The clear differences in the gas samples were been evident. While the cycled aged cell developed a kind of H_2/CO mixtures, the new cell produced a lot of H_2 without CO. The new cell was also produced a lot of C_2H_4, the other hydrocarbons were existing only in small concentration.

3.4 Exemplary celltest: cycled GA at 70 W oven performance

The cell test of the cyclically aged GA is shown in Figure 16.

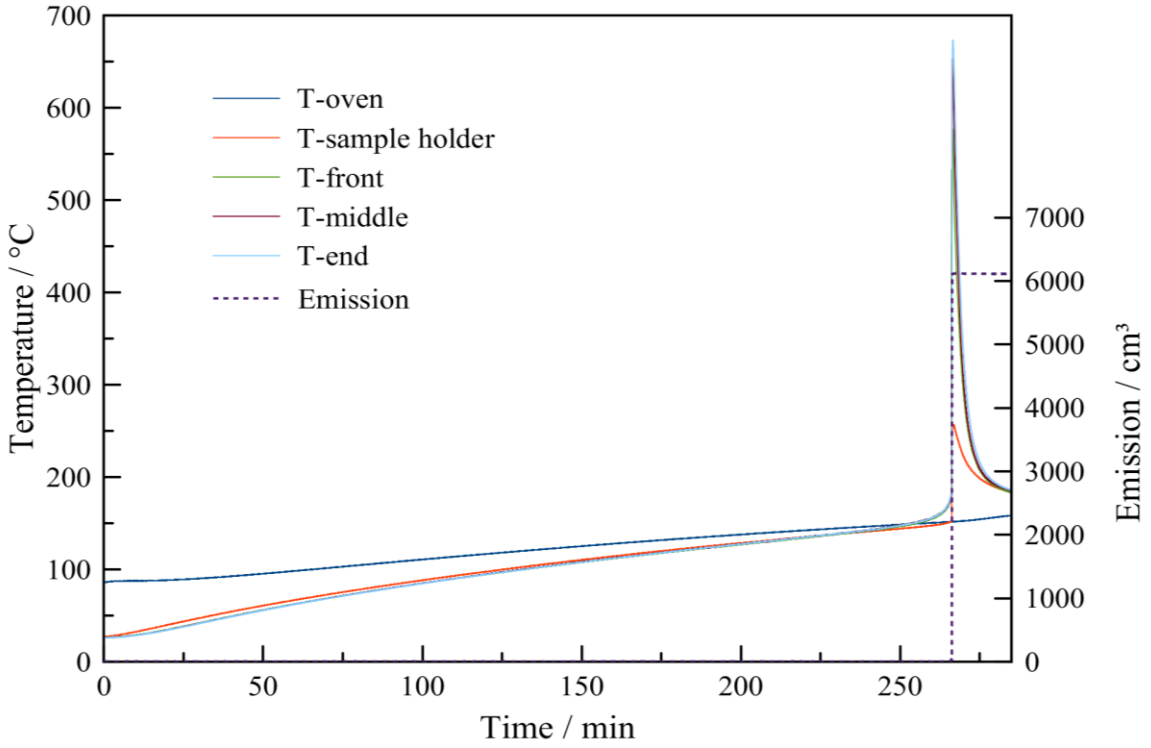

Figure 16: Temperature and emission over time of a cycling NCR18650GA cell (test: 11).

The temperature of the cell was slowly increased with the running test time, and exceeded the oven temperature after 250 minutes at a temperature of 157 °C. This was also the temperature at which the cell reached T_{TR}. After 265 min the thermal runaway occurred, which reached a maximum temperature of 663 °C. The cell did not show a venting event during the whole test period, thus the absolute emission of 6116 cm³ was achieved during the thermal runaway.

3.5 Exemplary celltest: new GA at 140 W oven performance

These experiments also used commercially purchased GA cells at test conditions of 140 W oven performance. Figure 17 shows the temperature and emission profile over time.

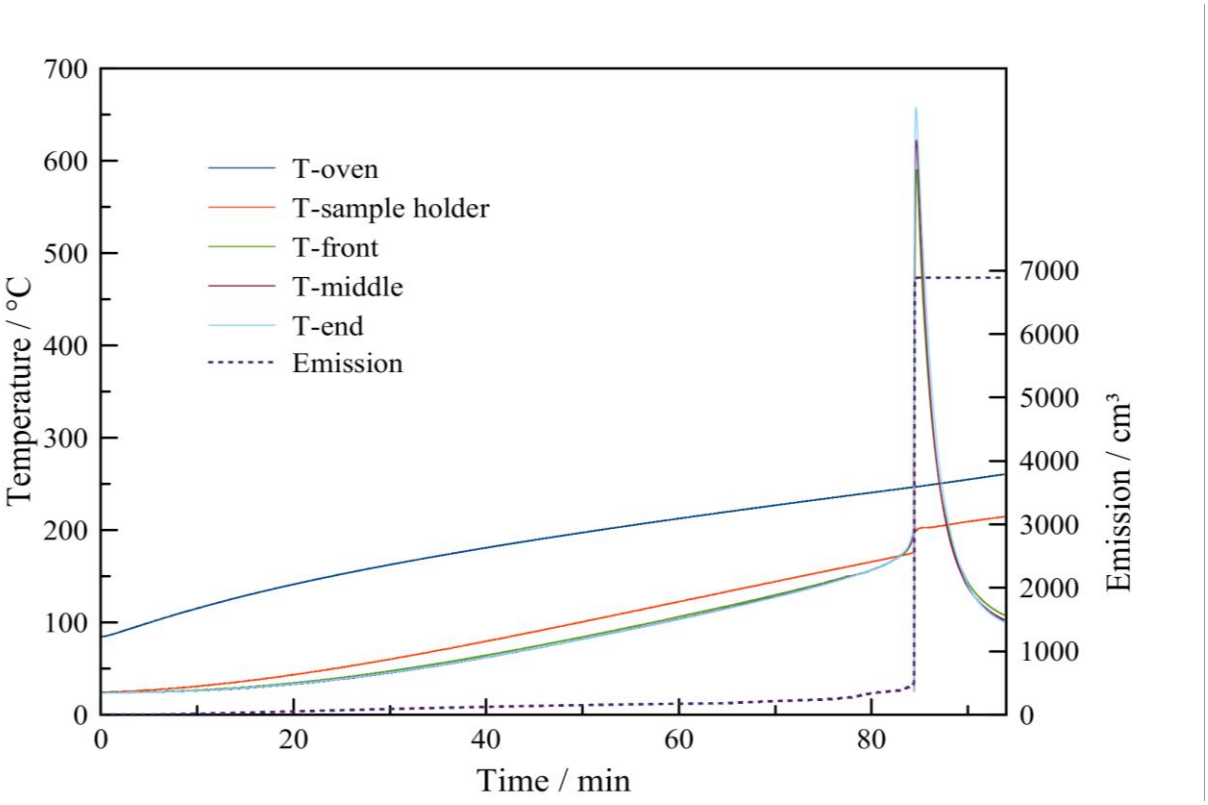

Figure 17: Temperature and emission over time of a new GA at 140 W oven performance (test: 13).

The 140 W furnace performance led to an expected rapid temperature increase of the cell and of the sample holder, where the temperature difference of the sample holder and the cell always was constant. From the temperature of 153 ° C (T_{TR}) a temperature increase of more than 4 °C/min was observable. The temperature difference between sample holder and cell got smaller because the cell became a heat source. After 84 min, the thermal runaway has taken place with a temperature of T_{max} = 657 °C. Again, no first venting event could be detected. Thereafter, the experiment was continued until no further changes were occurring. The thermal expansion and thermal runaway event produced an absolute gas volume of 6887 cm³ throughout the experiment.

3.6 Analysis of GA

2 new cells were tested under a heating ramp with 140 W and 2 cycled cells were tested under a ramp with 70 W. For a better comparability all data were filtered for the points of interest. The experimental results are summarized in Table 14.

Table 14: Summarized results of GA.

Experiment	m_{start} [g]	m_{end} [g]	Δm [g]	T_{vent} [°C]	T_{TR} [°C]	T_{max} [°C]	Emission [cm³]
11	46.79	28.32	18.47	-	157	673	6116.4
12	46.81	22.38	24.43	-	156	666	-
13	46.72	15.00	31.72	-	153	657	6887.9
14	46.92	21.32	21.46	-	159	620	-

The 1st venting events were not recognizable over the entire test series. This does not mean that these events have not taken place, but that they have only proceeded very creepingly.

With the definition of the T_{TR} for 140 W and 70 W experiments very similar results in the various GA tests could be observed. A difference between the new and cyclically aged cells was that the aged cells continuously released a small increasing amount of gas during the whole heating phase of the cell. The significant gas evolution happened during the thermal runaway event of the cells and again showed a good comparability of new and cyclically aged cells.

The next table (Table 15) offers the gas composition of the aged and new GA cells immediately after the thermal runaway.

Table 15: Gas composition of the different GA cells, each sample was taken immediately after the thermal runaway event.

Experiment	H_2 [%]	CH_4 [%]	CO [%]	CO_2 [%]	C_2H_4 [%]	C_2H_6 [%]	C_2H_2 [%]
12	25.64	5.17	49.29	18.74	0.84	0.14	0.20
14	28.69	4.90	47.23	18.30	0.76	0.13	0

The developed gases showed a small difference. The cycled GA cell developed more CO than the new one, this was also seen at the B cells. All hydrocarbons existed only in small concentration.

3.7 Exemplary celltest: calendrically aged VTC5A at 70 W oven performance

Figure 18 displays the temperature and gas emission profile over time of a calendrically aged VTC5A cell.

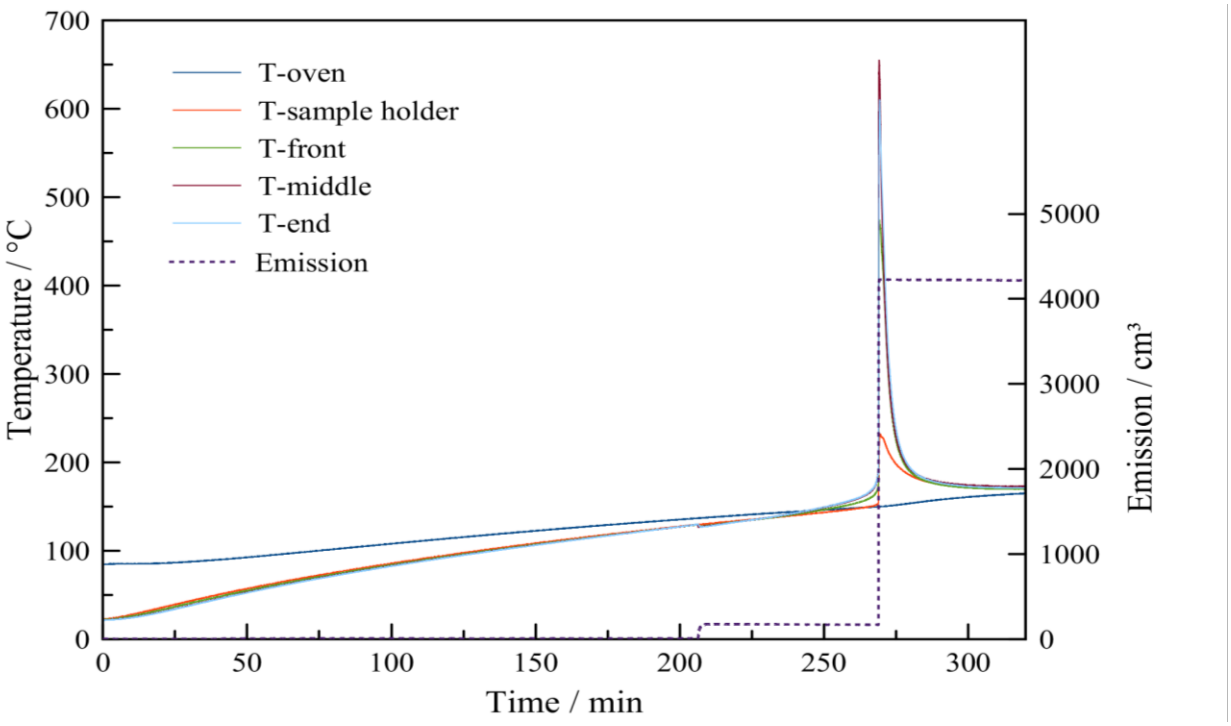

Figure 18: Temperature and emission over time of a calendrically aged VTC5A cell (test: 21).

The furnace temperature at the beginning of the experiment was approx. 80 °C and increased continuously on a heat ramp of 70 W by the DC power supply. The cell and the sample holder started at 24 °C and approached the oven temperature. The cell vented at a cell temperature of 129 °C with a temperature drop of ≈ 4 °C. After the first venting, the cell temperature began to rise again with increasing rate. At a cell temperature about 136 °C the cell temperatures exceeded the oven temperature. At a cell temperature of 162 °C the cell reached the thermal onset temperature (starting about 2 °C/min, T_{TR}). The temperature climbed sharply, which was also led to rapid heating of the sample holder.

After reaching of T_{TR}, the cell got into a thermal runaway. A temperature of 655 °C (T_{max}) was reached. In combination with the 1st venting event and thermal runaway, an absolute gas volume of 4227 cm³ was generated during the experiment. Thereafter, the experiment was continued until the cell temperatures approached the temperature values of the furnace over a longer period of time and no further changes were expected.

3.8 Exemplary celltest: new VTC5A at 140 W oven performance

The results of the cell tests for the US18650VTC5A cells are plotted in Figure 19.

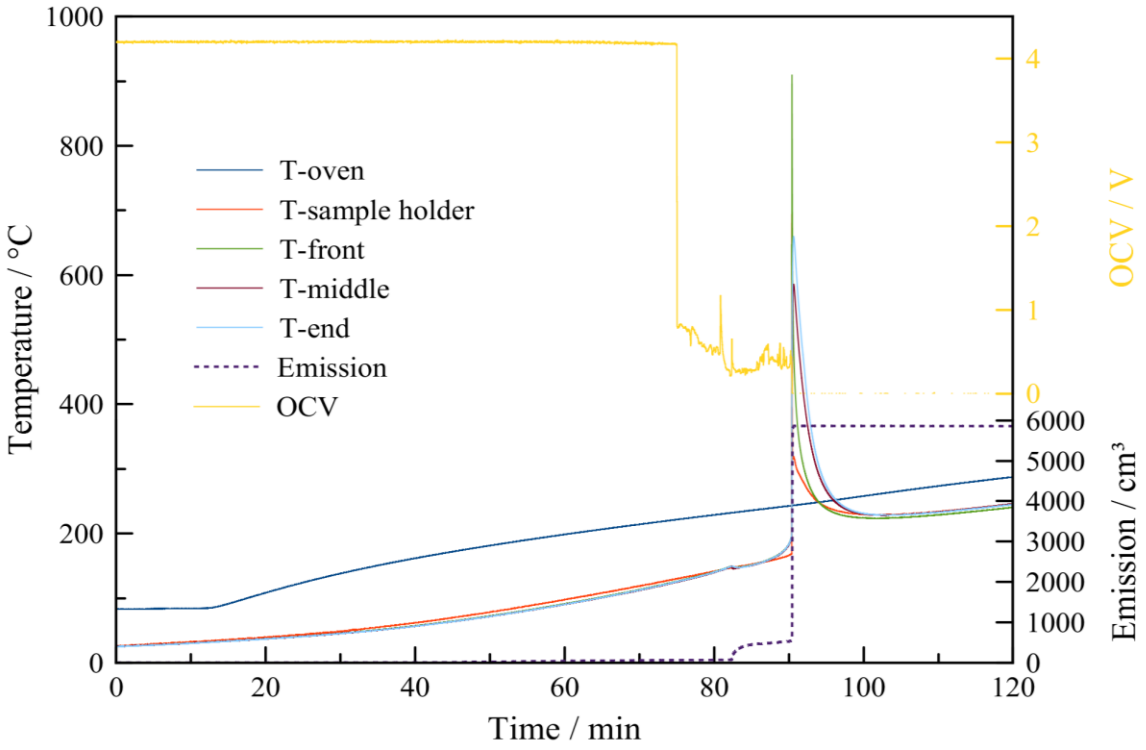

Figure 19: Temperature, emission and voltage plot of a new VTC5A cell at 140 W oven performance (test: 23).

For the first 73 min the OCV showed a constant value of 4.2 V and then the voltage curve spontaneously fell to 0.8 V. In the further course, the voltage fluctuated between 1 and 0.4 V. When the cell went into the thermal runaway the OCV dropped to 0 V when and no further voltages were measured.

The 140 W oven performance led to an expected rapid temperature increase of the cell and of the sample holder. The 1st venting occurred after 83 min at 149 °C. From the temperature of 153 °C (T_{TR}) a continuous temperature increase of more than 4 °C/min was observable. After 84 min, the thermal runaway has taken place at a maximum temperature of 659 °C (T_{max}). The thermal expansion, the 1st venting and thermal runaway event produced an absolute gas emission of 5863 cm³ during the experiment. Thereafter, the experiment was continued until no further changes were expected.

3.9 Analysis of VTC5A

2 new cells with 140 W and 2 calendrically aged cells with 70 W oven performance were tested. For a better comparability were all data filtered out for only the points of interest. These experimental results are summarized in Table 16.

Table 16: Summarized results of VTC5A.

Experiment	m_{start} [g]	m_{end} [g]	Δm [g]	T_{vent} [°C]	T_{TR} [°C]	T_{max} [°C]	Emission [cm³]
21	47.53	27.21	20.32	129	162	655	4227.5
22	47.51	29.38	18.13	132	161	638	-
23	47.27	22.37	24.90	149	153	659	5863.9
24	47.25	21.58	25.67	148	152	657	-

There were small differences in the initial weight between the new and calendarically aged cells. Furthermore, the 1st venting event of the calendarically aged cells had been much earlier than of the new ones. Also the beginning of the exothermic phase occurs later in the case of the calendrically aged cells. The peak values of the thermal runaway (T_{max}) were very similar. From this and from the gas emissions results it can be concluded that the new cells were more resistant to temperature than the aged ones.

The next table (Table 17) shows the gas composition of the cycling aged and new GA cells immediately after the thermal runaway.

Table 17: Gas composition of the different VTC5A cells, each sample was taken immediately after the thermal runaway event.

Experiment	H_2 [%]	CH_4 [%]	CO [%]	CO_2 [%]	C_2H_4 [%]	C_2H_6 [%]	C_2H_2 [%]
22	16.63	2.63	53.46	24.17	0	3.04	0.07
24	73.14	16.29	0	0	1.71	7.97	0.9

The developed gases of the VTC5A experiments have shown an explicit difference. The calendarically aged VTC5A cell has produced a lot of CO. This was comparable with the cycling aged cell B and GA. The CO and CO_2 values from experiment 24 were 0%, which could be, because the values were so small that these were lost during the preparation from the initial program to the table.

3.10 Exemplary celltest: calendrically aged HE4 at 70 W oven performance

The calendarically aged HE4 cell has been very resistant. No thermal runaway happened until 200 °C at 70 W oven performance. Figure 20 displays the temperature and gas emission profile over time by using the stronger AC heater device.

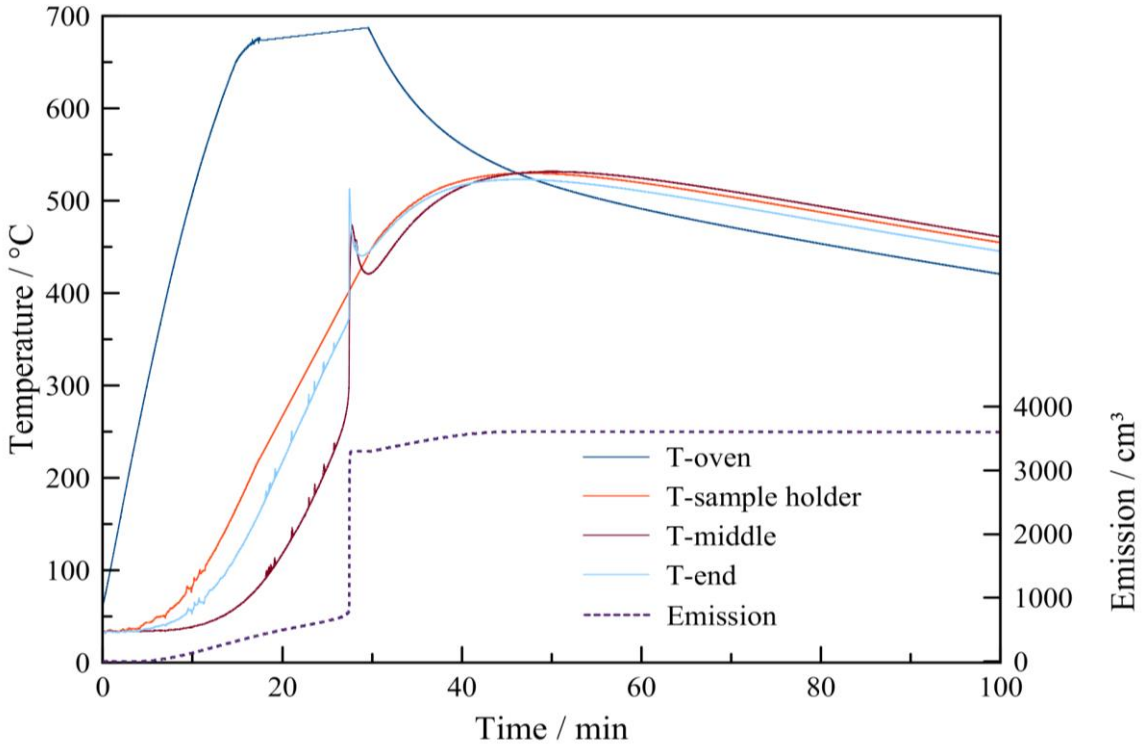

Figure 20: Temperature and emission over time of a calendarically aged HE4 cell (test: 31).

Therefore the AC device was connected and the furnace was heated to 700 °C to ensure full break-down. The initial conditions were the oven temperature at 80 °C and the cell and sample holder temperature at 24 ° C. The heating rate was too large; no first venting and onset temperature were located. From the start could be seen a constantly rising gas emission, which is due to the strong heating rate and expansion of the inert gas. After 27 minutes a significant emission occurred, which symbolizes the thermal runaway with a peak temperature of 512 °C (T_{max}). The total gas emission from this experiment was about 3601cm³.

3.11 Exemplary celltest: new HE4 at 140 W oven performance

The results of the cell tests for the HE4 are plotted in Figure 21.

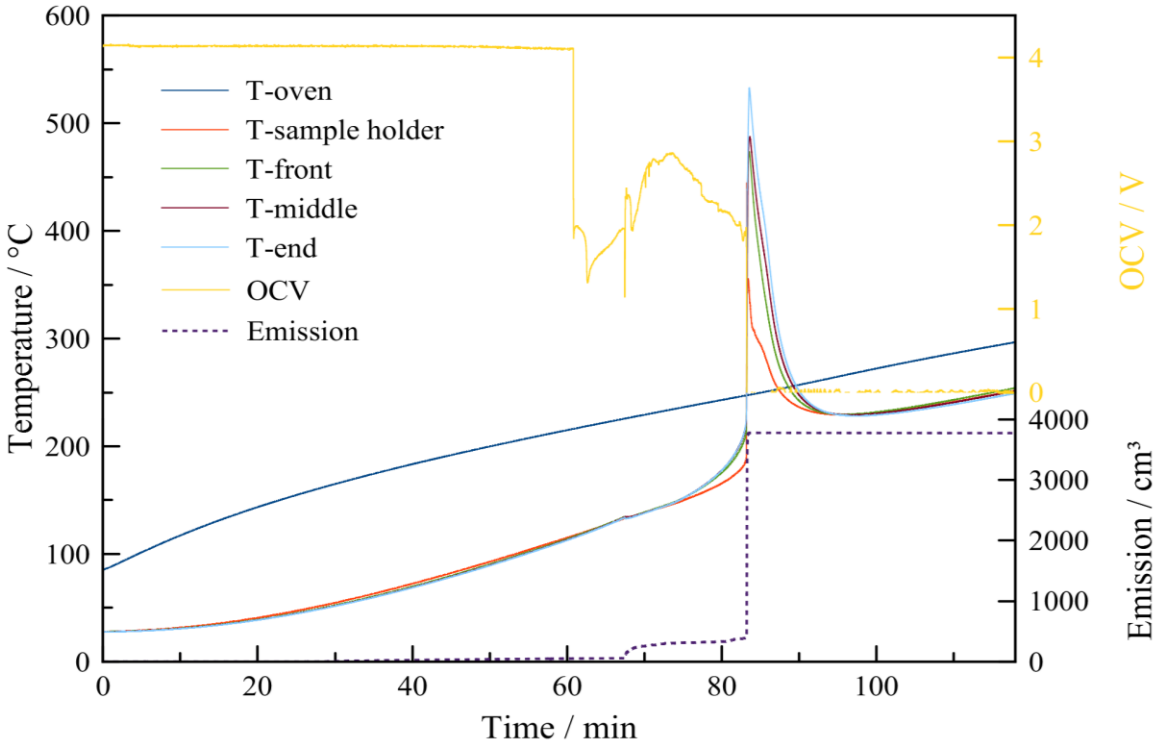

Figure 21: Temperature, emission and voltage plot of a new HE4 cell by 140 W oven performance (test: 33)

The new HE4 cells showed a constant OCV value of 4.17 V for the first 59 min until a cell temperature of 99 °C, and then the voltage curve spontaneously fell to 1.8 V. In the further course, the voltage fluctuated between 3 and 1.4 V, only at a cell temperature of 133 °C the voltage was dropped temporarily from 1.9 to 1.1 V. At 133 °C also the 1st venting event occurred. At 148 °C the cell temperature rate rose over 4 °C/min (T_{TR}). When the cell went into the thermal runaway with a maximal temperature of 532 °C (T_{max}) the OCV dropped to 0 V and a total gas emission of 3777 cm³ was produced.

3.12 Analysis of HE4

From the HE4 2 new cells with an oven performance of 140 W and 2 calendrically aged cells at 70 W were tested. In the following table (Table 18) all data is filtered for the points of interest.

Table 18: Summarized results of HE4.

Experiment	m_{start} [g]	m_{end} [g]	Δm [g]	T_{vent} [°C]	T_{TR} [°C]	T_{max} [°C]	Emission [cm^3]
31	45.51	26.01	19.50	-	-	512	3601.1
32	45.51	26.81	18.70	-	-	519	3009.7
33	45.42	26.73	18.79	133	148	532	3777.5
34	45.55	22.02	23.53	135	148	493	-

In the case of the calendarically aged cells, no first venting event and no beginning of the exothermic phase could be noted. The peak temperatures at the thermal runaway were around 500 °C with a gas emission about 3500 cm^3. For the new cells the thermal runaway temperature and gas emission was very similar. But the new cells have shown a 1st venting at 133 °C and a thermal runaway temperature at 148 °C (T_{TR}).

The next table (Table 19) shows the gas composition of all HE4 cells immediately after the thermal runaway.

Table 19: Gas composition sample of HE4, the sample was taken immediately after the thermal runaway event.

Experiment	H_2 [%]	CH_4 [%]	CO [%]	CO_2 [%]	C_2H_4 [%]	C_2H_6 [%]	C_2H_2 [%]
34	33.86	3.57	34.83	24.96	2.54	0.24	0

In the case of experiment 32 the stronger AC heater device was used to get the cell into a thermal runaway. During the experiment with the calendarically aged HE4 cell (experiment 32) with the AC device, no sampling was carried out, because the comparability between experiments, which used the stronger AC heater device than the weaker DC device, was not given. The developed gases of the new HE4 (experiment 34) has shown an equal distribution of the produced compounds. Only methane and C_2H_4 were detected to approximate 2%. C_2H_6 was detected in very small concentration. C_2H_2 was not present.

3.13 Exemplary celltest: cycled 35E at 70 W oven performance

Figure 22 displays the temperature and gas emission profile over time of a cycled 35E cell.

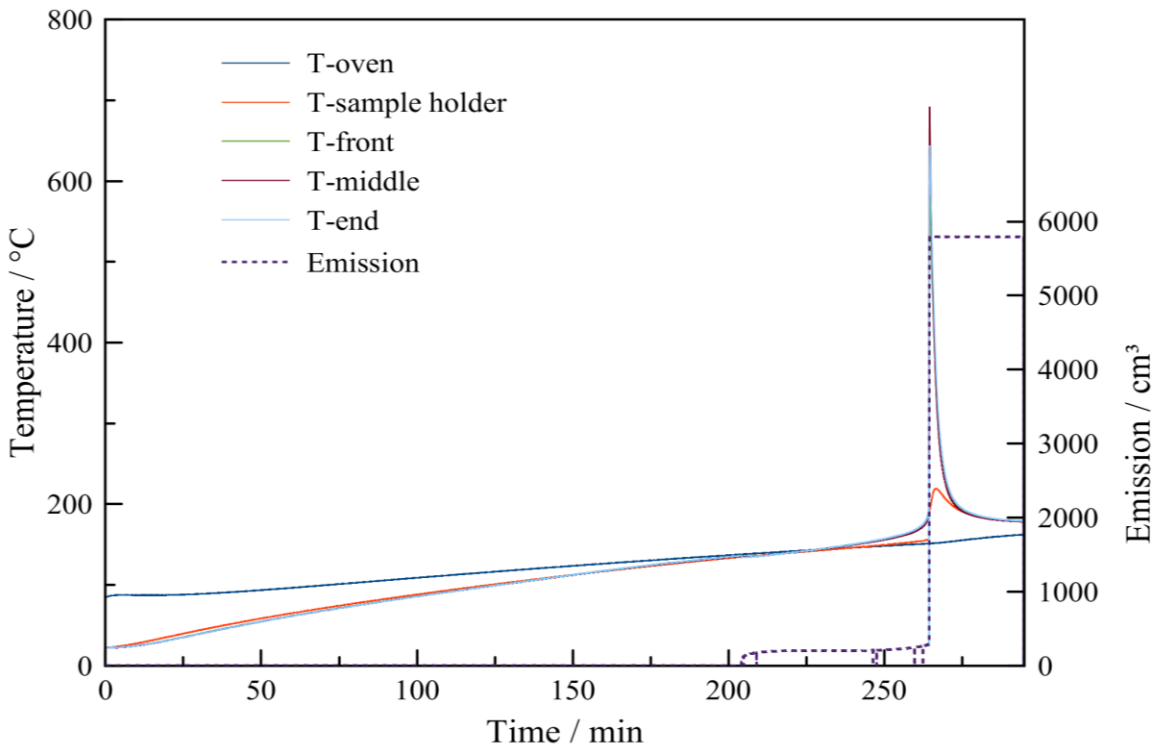

Figure 22: Temperature plot of a cycling 35E cell (test: 41).

The temperature of the cell was slowly increased with the running test time, and exceeded the oven temperature after 220 minutes at a temperature of 142 °C. At the temperature 136 °C occurred the 1st venting and at 167 °C (T_{TR}) the cell became a heating source. Shortly after the exothermic start it came to the thermal runaway, which reached a maximum temperature of 691 °C. During the thermal runaway the cell released a gas emission of 5795 cm³.

3.14 Exemplary celltest: calendrically aged 35E at 70 W oven performance

The calendrically aged 35E's temperature, gas emission and voltage over time plot were shown in Figure 23.

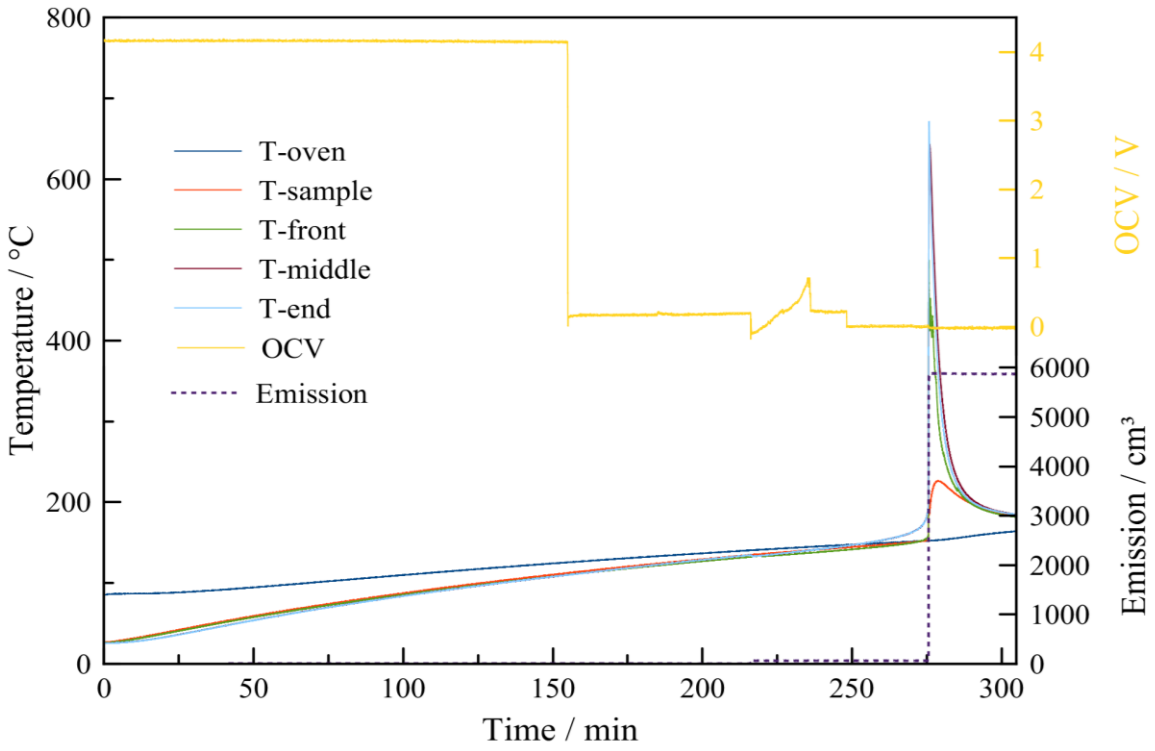

Figure 23: Temperature, gas emission and voltage over time of a calendarically aged 35E cell (test: 43).

The experiment starts with an oven temperature about 80 °C, a cell and sample holder temperature at 24 °C and an OCV of 4.1 V. Already after 152 min the OCV droped irrepealably to 0 V. The cell vented at a cell temperature of 136 °C with a temperature drop of ≈ 2 °C. After the first venting, the cell temperature began to rise again with increasing rate. At a cell temperature of about 167 °C the cell temperature exceeded the oven temperature. At a cell temperature of 163 °C the cell reached the thermal runaway temperature (T_{TR}). Shortly after reaching T_{TR}, the cell got into a thermal runaway. A peak temperature of 642 °C (T_{max}) was reached. In combination with the 1st venting event and thermal runaway, an absolute gas volume of 5878 cm³ was generated during the experiment. The experiment was continued until no further changes were expected.

3.15 Exemplary celltest: new 35E by 140 W oven performance

The results of the new 35E cells are plotted in Figure 24.

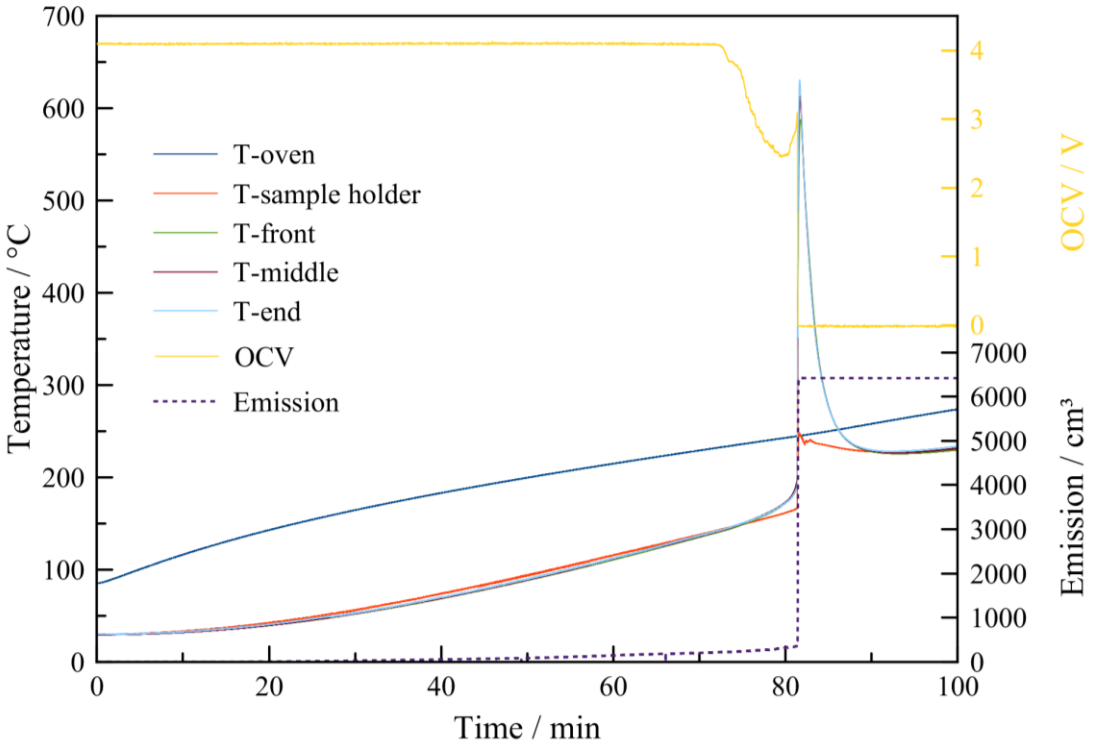

Figure 24: Temperature, gas emission and voltage plot of a new 35E cell by 140 W oven performance (test: 45).

The new 35E cells was shown a constant OCV value of 4.1 V for the first 71 min until a cell temperature of 130 °C, it was estimated that the 1st venting was occurred at this point. Then the voltage curve was slowly fallen to 2.4 V. For the thermal runaway the voltage was increase to 3.3 V. At 133°C was the cell temperature where the 1st venting event was occurred. At 153 °C the cell temperature rate was became over a rate of 4 °C (T_{TR}). When the cell got into the thermal runaway with a maximal temperature of 532 °C (T_{max}) the OCV dropped to 0 V and a total gas emission of 6420 cm³ was produced.

3.16 Analysis of 35E

The 35E test series consisted of 2 cyclically aged, 2 calendrically aged and 2 new cells. In the following table (Table 20) all data are filtered for the points of interest.

Table 20: Summarize results of 35E

Experiment	m_{start} [g]	m_{end} [g]	Δm [g]	T_{vent} [°C]	T_{TR} [°C]	T_{max} [°C]	Emission [cm³]
41	47.65	24.73	23.69	136	167	691	5795.4
42	47.66	24.61	23.05	136	170	716	-
43	47.66	31.72	16.24	134	163	642	5878.4
44	47.63	31.42	20.50	136	162	706	-
45	47.47	20.97	26.50	142	153	612	6420.1
46	47.62	20.02	27.60	143	151	578	-

It can be seen that the experiments 41 – 44 performed very similar. In the case of experiment 45 and 46, the first venting event took place 10 °C before and the beginning of the exothermic phase took place 10 °C after the aged cells. The peak temperatures at the thermal runaway were at 700 °C for the aged cells and around 600 °C for the new ones. The gas emission of the aged cells was 600 cm³ lower than of the new cells.

The next table (Table 21) shows the gas composition of all 35E immediately after the thermal runaway.

Table 21: Gas composition of the different 35E cells, each sample was taken immediately after the thermal runaway event.

Experiment	H_2 [%]	CH_4 [%]	CO [%]	CO_2 [%]	C_2H_4 [%]	C_2H_6 [%]	C_2H_2 [%]
42	21.96	4.16	52.91	18.60	1.92	0.13	0.28
44	23.04	8.18	52.72	13.77	2.01	0.07	0.21
46	68.15	0	22.75	9.11	0	0	0

Even the previous experiments of aged cells showed that, the aged cells produced a lot of CO during the thermal runaway event (see experiment 42 and 44). Hydrocarbons were detected in the vent gas from the aged cells. In contrast the new cell produced no hydrocarbons.

3.17 Exemplary celltest: cycled MJ1 at 70 W oven performance

The following figure (Figure 25) displays the temperature and gas emission profile of a cycling MJ1 over time.

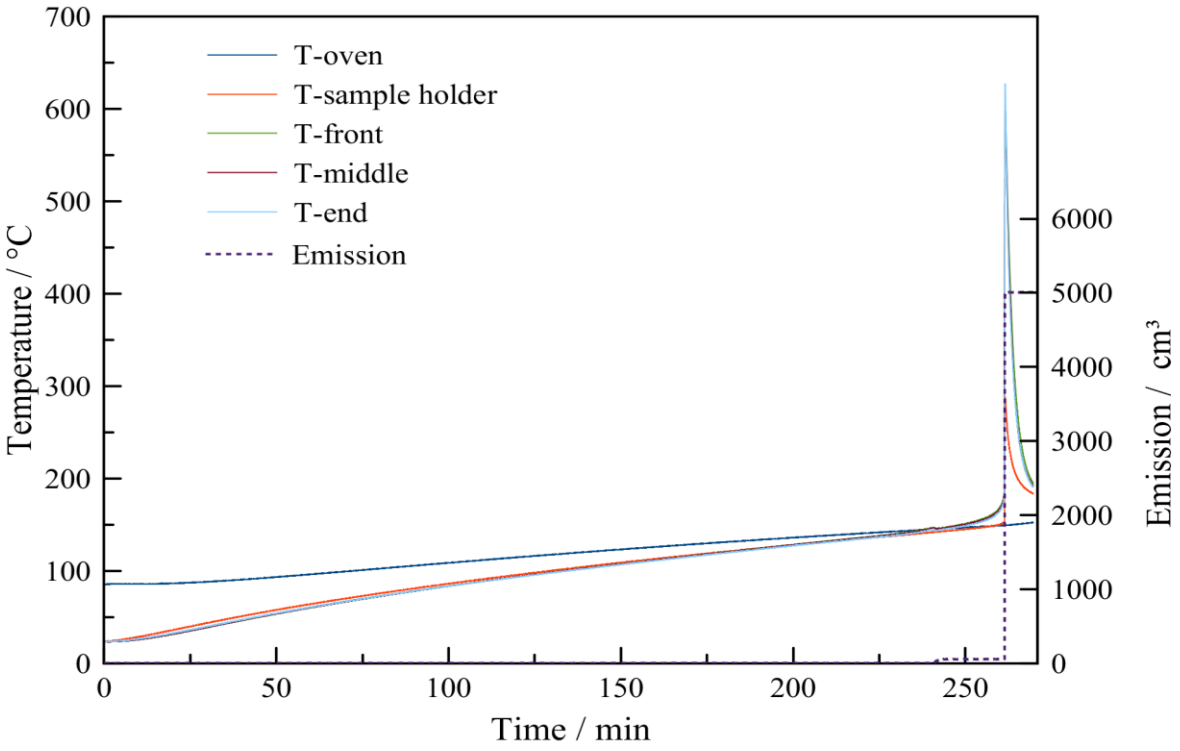

Figure 25: Temperature plot of a cycled MJ1 cell (test: 51)

The temperature of the cell slowly increased with the running test time, and exceeded the oven temperature after 229 minutes at a temperature of 147 °C. The 1st venting occurred at cell temperature of 141 °C and at 167 °C (T_{TR}) the cell became into the exothermic phase. Shortly after the exothermic start, it came to the thermal runaway, which reached a maximum temperature of 627 °C. The cell produced a gas emission of 5008 cm³ during the thermal runaway.

3.18 Exemplary celltest: calendrically aged MJ1 at 70 W oven performance

The calendrically MJ1 temperature, gas emission and voltage over time plot are shown in Figure 26.

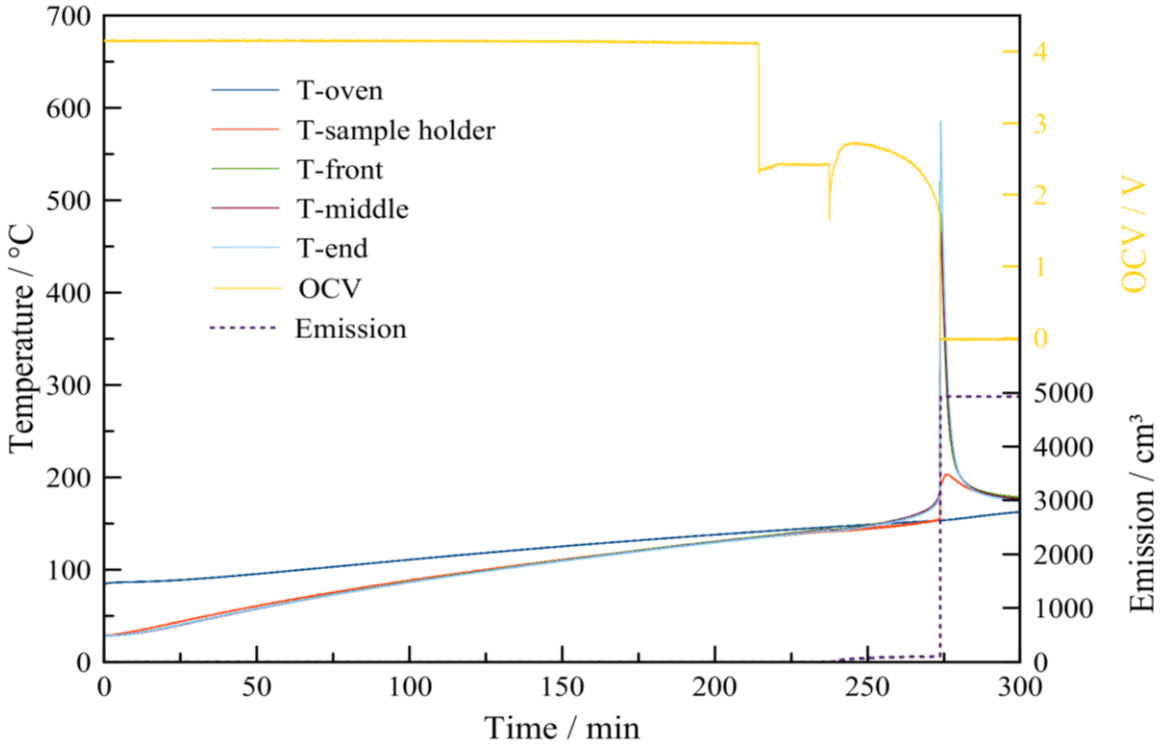

Figure 26: Temperature, gas emission and voltage over time of a calendaring aged MJ1 cell (test: 53).

The experiment starts with an oven temperature of about 80 °C, a cell and sample holder temperature at 24 °C and an OCV of 4.12 V. After 212 min the OCV drops to 2.4 V. The cell vented at a cell temperature of 136 °C with a temperature drop of ≈ 2 °C. At this point the OCV decreased to 1.6 V and then recovered to 2.75 V. After the first venting, the cell temperature began to rise again with an increasing rate. At a cell temperature about 169 °C, the cell temperatures exceeded the oven temperature. At a cell temperature of 162 °C the cell reached the thermal runaway temperature (T_{TR}). Shortly after hitting T_{TR}, the cell got into a thermal runaway. A peak temperature of 585 °C (T_{max}) was reached. In combination with the 1st venting event and thermal runaway, an absolute gas volume of 4931 cm³ was generated during the experiment. The experiment was continued until no further changes were expected.

3.19 Exemplary celltest: new MJ1 by 140 W oven performance

The results of the new MJ1 cells are plotted in Figure 27.

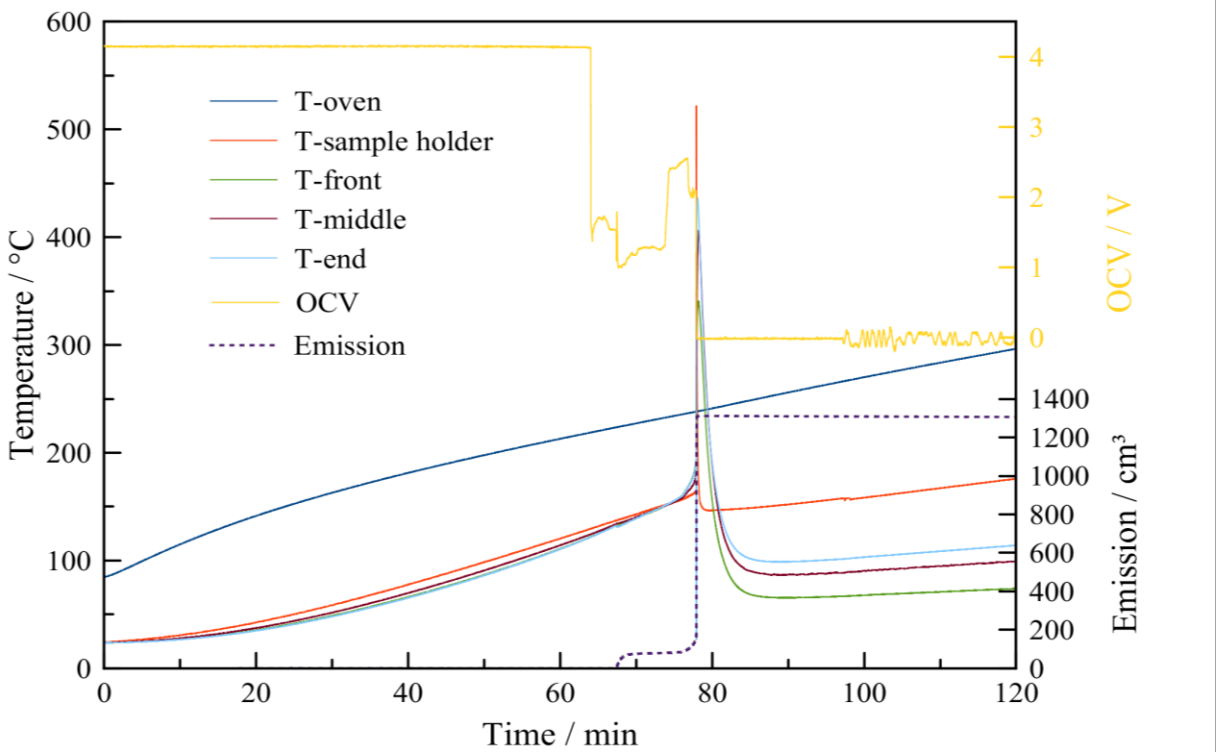

Figure 27: Temperature, emission and voltage plot of a new MJ1 cell by 140 W oven performance (test: 56).

The new MJ1 showed a constant OCV value of 4.11 V for the first 62 min until a cell temperature of 115 °C. After that, the voltage varied between 2.5 and 0.9 V. The 1st venting was occurred 139 °C. At 154 °C, the cell heating rate rose over a rate of 4 °C/min (T_{TR}). When the cell went into the thermal runaway with a maximal temperature of 521 °C (T_{max}) the OCV was dropped to 0 V and a total gas emission of 1310 cm³ was produced.

3.20 Analysis of MJ1

The MJ1 test series consisted of 2 cycling, 2 calendrical and 2 new cells. In the following table (Table 22) all data are filtered for the points of interest.

Table 22: Summarized results of MJ1.

Experiment	m_{start} [g]	m_{end} [g]	Δm [g]	T_{vent} [°C]	T_{TR} [°C]	T_{max} [°C]	Emission [cm³]
51	45.72	17.77	27.95	143	155	627	5008.8
52	45.67	14.76	30.91	144	156	523	-
53	45.62	17.93	27.69	141	162	585	4931.4
54	45.65	20.97	24.68	142	165	606	-
55	46.31	9.35	36.99	141	153	504	-
56	46.34	8.81	37.50	131	152	521	1310.5

It can be seen again that the cyclically and calendrically aged cells acted very similar. The cycled and new cells started their respective exothermic phase at a cell temperature about 155 °C, while the calendarically aged cells began to react at 165 °C. The peak temperatures at the thermal runaway were at 600 °C for the aged cells and around 500 °C for the new ones. In contrast was the gas emission of the aged cells at 5000 cm³ and about 1300 cm³ for the new cells.

The next table (Table 23) shows the gas composition of all MJ1 immediately after the thermal runaway.

Table 23: Gas composition of the different MJ1 cells, each sample was taken immediately after the thermal runaway event.

Experiment	H_2 [%]	CH_4 [%]	CO [%]	CO_2 [%]	C_2H_4 [%]	C_2H_6 [%]	C_2H_2 [%]
52	33.28	7.50	32.85	24.58	1.49	0.21	0.10
54	33.87	7.83	36.93	18.98	2.20	0.19	0
55	24.62	5.80	51.22	16.36	1.82	0.17	0

In contrast to the other experiments produced the new MJ1 a lot of CO. All MJ1 released nearly the same H_2/CO mixture gas concentration and the hydrocarbons in all samples were only present in traces.

3.21 Exemplary celltest: iPhone battery

The temperature, gas emission and OCV experiment with the iPhone 6S cell are plotted in Figure 28.

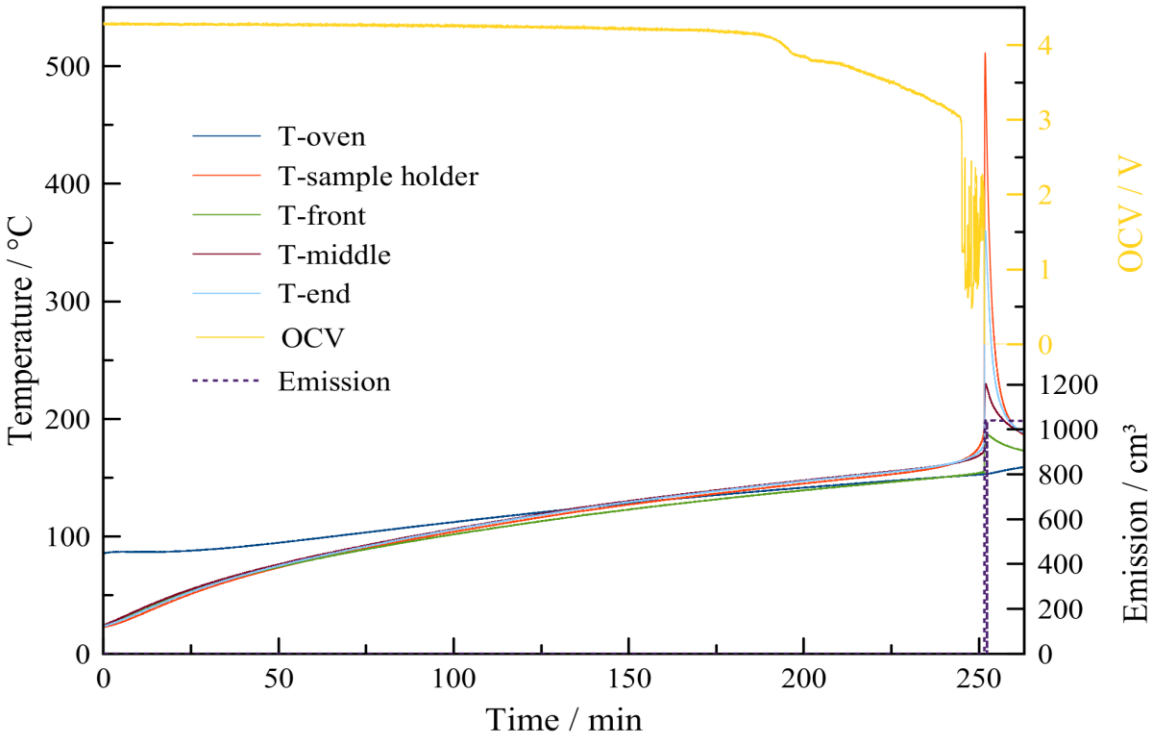

Figure 28: Thermal ramp test pot from an iPhone 6S battery; temperature, gas emission and OCV over time (test: 61).

The experiment starts under the same conditions as the 18650 cells. An oven temperature of about 80 °C, a cell and sample holder temperature at 24 °C and an OCV of 4.11 V mark the start of the test. The cell and sample holder temperature was approached the oven temperature. After 145 min the OCV gradually decreased. No first venting event was identified in this experiment. After 136 min the cell temperature was nearly the same as the oven temperature. After 152 min the cell exceeded the oven temperature at 142 °C. At reaching T_{TR} = 166 °C, the cell got into a thermal runaway. A peak temperature of 511 °C (T_{max}) was reached. At this point an absolute gas volume of 1039 cm³ was generated. The experiment was continued until no further changes were expected.

3.22 Analysis of iPhone

The iPhone 6S cell test series consisted of 5 experiments. In the following table (Table 24) data regarding the points of interest is shown.

Table 24: Summarized results of the iPhone 6S battery.

Experiment	m_{start} [g]	m_{end} [g]	Δm [g]	T_{vent} [°C]	T_{TR} [°C]	T_{max} [°C]	Emission [cm³]
61	25.21	21.09	4.12	-	166	511	1039.1
62	25.19	23.36	1.83	-	-	-	-
63	25.18	23.45	1.73	-	-	-	-
64	25.18	21.08	4.10	-	167	683	-
65	25.17	22.91	2.26	-	-	-	-

It can be seen that only the experiments 61 and 64 have exhibited a thermal runaway event. The thermal runaway temperatures of these experiments were comparable with each other, but the experiment 64 led to a significantly higher maximal temperature during the thermal runaway.

The next table (Table 25) shows the gas composition of the iPhone cells. Each sample was taken at the estimated point, where the thermal runaway should have been.

Table 25: Gas composition of the iPhone 6S battery, each sample was taken at the estimated point of temperature, where the thermal runaway should have been.

Experiment	H_2 [%]	CH_4 [%]	CO [%]	CO_2 [%]	C_2H_4 [%]	C_2H_6 [%]	C_2H_2 [%]
62	1.57	1.16	1.82	90.36	4.36	0.74	0
63	2.31	1.96	3.59	84.55	6.56	1.04	0

A thermal runaway event could not be recorded at a gas sample experiment. Nevertheless, traces of hydrocarbons and other compounds could be determined.

3.23 Exemplary celltest: SGS6

The Samsung Galaxy S6 battery cells have been very resistant. No thermal runaway was happening in the SGS6 cell until 200 °C by 70 W oven performance with the DC heating device. Figure 29 displays the temperature, gas emission and OCV profile over time. By using the stronger AC heating device to push the SGS6 cell to its limit.

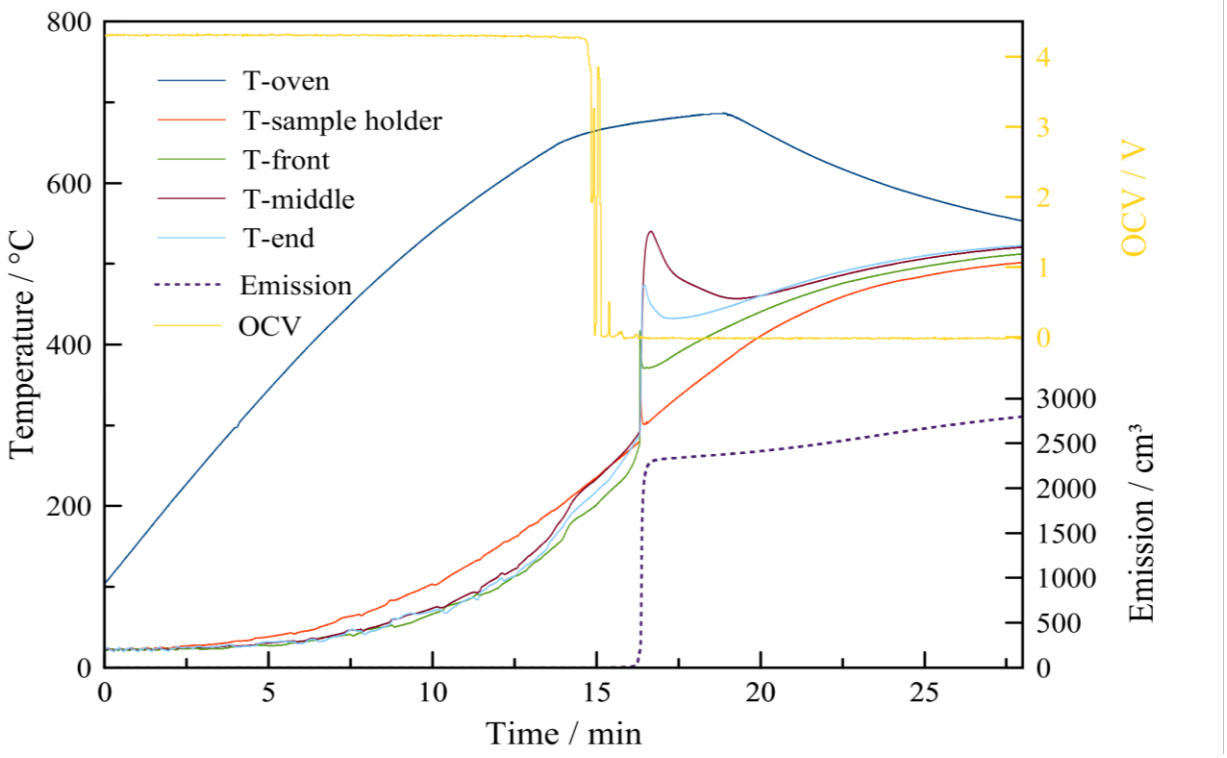

Figure 29: Thermal ramp test pot from Samsung Galaxy S6 battery; temperature, gas emission and OCV over time (test: 75).

For stronger stress testing the AC device was connected and used to heat to an oven temperature to 700 °C. The initial conditions were the oven temperature at 80 °C and the cell and sample holder temperature at 24 °C. The strong heating rate was too large to detect the first venting, onset temperature and thermal runaway begin (T_{TR}). After 16 minutes a significant emission occurred which indicated the thermal runaway with a peak temperature of 540 °C (T_{max}). The total gas emission from this experiment was about 2321 cm³.

3.24 Analysis of SGS6

The SGS6 cell test series consisted of 5 experiments (see Table 26).

Table 26: Summarized results of the Samsung Galaxy S6 battery.

Experiment	m_{start} [g]	m_{end} [g]	Δm [g]	T_{vent} [°C]	T_{TR} [°C]	T_{max} [°C]	Emission [cm^3]
71	33.19	31.19	2.00	-	-	-	-
72	33.18	31.22	1.96	-	-	-	-
73	33.21	30.91	2.30	-	-	-	-
74	33.18	30.63	2.55	-	-	-	-
75	33.18	25.45	7.73	-	213	540	2321.2

It can be seen that only the experiment V05 showed a thermal runaway event. This could only be accomplished by the strongly heating of the AC device. An exothermic onset start temperatures could be located by 213 °C.

Table 27 shows the gas composition of the SGS6. Each sample was taken at the estimated temperature, at which the thermal runaway could have happened. This was done because there was no thermal runaway event as with the other cell types. So samples were taken continuously at equal time intervals throughout the whole experiment. These remain constant time intervals deliver at all samples similar results. For this reason only the gas composition at which the thermal runaway event has estimated, was introduced in Table 27.

Table 27: Gas composition of the Samsung Galaxy S6 battery, each sample was taken at the estimated point of temperature, at which the thermal runaway could have been.

Experiment	H_2 [%]	CH_4 [%]	CO [%]	CO_2 [%]	C_2H_4 [%]	C_2H_6 [%]	C_2H_2 [%]
72	1.03	0.93	0	90.81	0	7.23	0
73	5.18	1.07	2.33	88.81	0	2.61	0

A thermal runaway event could not be recorded at a gas sample experiment. There could be determined traces of hydrocarbons and other compounds and a lot of CO_2.

3.25 Exemplary celltest: new LG G3

The results of the LG cells are plotted in Figure 30.

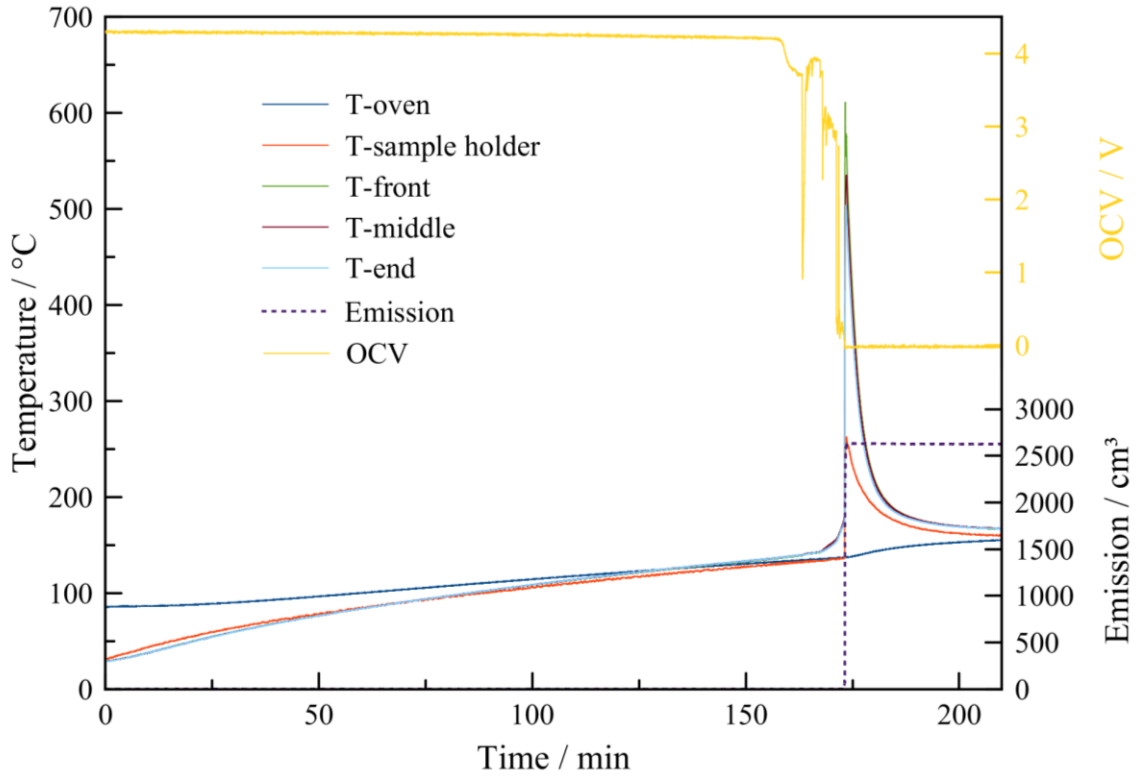

Figure 30: Thermal ramp test pot from an LG G3 battery; temperature, gas emission and OCV over time (test: 81).

The experiment was started under typical conditions. The OCV value was constant over a long period of heating at 4.14 V. After 159 min, the OCV started to fluctuate. A first venting event did not occur. After reaching of T_{TR} at 246 °C, the cell went into a thermal runaway and the voltage dropped to zero. A peak temperature of 489 °C (T_{max}) was reached in combination with an absolute gas emission of 2940 cm³. The experiment was continued until no further changes were expected.

3.26 Analysis of LG G3

The LG cell series consisted of 5 experiments. In Table 28 all data of interest are summarized.

Table 28: Summarized results of the LG G3 battery.

Experiment	m_{start} [g]	m_{end} [g]	Δm [g]	T_{vent} [°C]	T_{TR} [°C]	T_{max} [°C]	Emission [cm^3]
81	46.98	37.59	9.39	-	145	489	2940.2
82	46.99	34.51	12.48	-	143	804	-
83	46.98	36.72	10.26	-	144	651	-
84	44.79	36.41	8.38	-	142	611	2630.7
85	45.22	31.72	13.50	-	146	424	-

There were differences in the initial weight, because in the first three experiments the short circuit, overvoltage and overheat protection were not removed before the tests. The 1st venting events were not recognizable over the entire test series. The evolution of gas could just have inflated the cell until the point of cell rupture during the thermal runaway.

In all cases, the T_{TR} temperatures were similar, but the maximum thermal runaway temperatures varied widely. This could be due to the detachment of the thermocouples during inflation of the cell, measurement of the temperature directly on the cell during the thermal runaway event thus is limited.

Table 29 shows the gas composition of the LG cells immediately after the thermal runaway event.

Table 29: Gas composition of the different B cells, each sample was taken immediately after the thermal runaway event.

Experiment	H_2 [%]	CH_4 [%]	CO [%]	CO_2 [%]	C_2H_4 [%]	C_2H_6 [%]	C_2H_2 [%]
82	30.69	11.58	6.81	36.35	13.06	1.06	0.44
83	30.91	8.11	0.07	49.01	10.62	0.89	0.38

The samples showed very similar results. Both experiment cells developed a lot of CO_2 and H_2 during the thermal runaway process. Also could be seen that much C_2H_4 was produced, the concentration of C_2H_6 and C_2H_2 were also larger than in all other experiments.

3.27 Summary of results

The open circuit voltage showed a diverse behavior for the different cell types. Beginning at 100 °C, all cells showed a decrease of the open circuit voltage. Fluctuations of the cell voltage could be observed after the first drop of the voltage.

Another strong decrease of the cell voltage could be seen during the first venting event of the cells, except the 35E or HE4 cells, which showed a slow increase of the cell voltage after the venting event. In all experiments regarding the GA, the calendrically aged HE4 and smartphone cells no first venting was indicated in the thermal behavior, but the gas analysis showed a significant amount of CO_2 before the thermal runaway. This indicates that a reaction occurred, which also was accompanied by an opening of the cell.

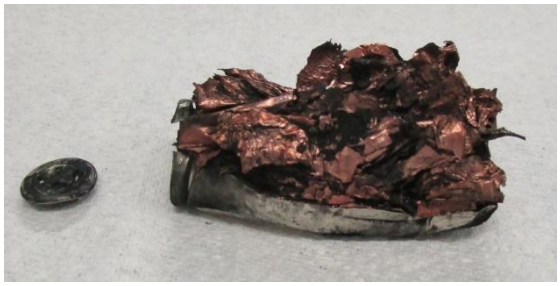

Figure 31: destroyed HE4 cell

Figure 32: destroyed LG cell

All cells were structurally damaged during the thermal runaway (see Figure 31 and Figure 32 and compare with Figure 8 and Figure 9). Investigations of the cells after the thermal runaway have shown a melting of the positive electrode's current collector. The aluminum from the positive electrode has a melting point of 660°C. It was visible in the post-mortem observation as small solidified metal droplets. The copper current collector of the negative electrode has a melting point of 1085 °C and did not melt under the test conditions.

The total emitted gas volume after the thermal runaway ranged from 1039 cm^3 to 6888 cm^3, depending on the cell type. Additionally it was experimentally proven that a higher heating performance of the oven leads to an increase of the gas emissions of the whole experiment.

The gas samples after the thermal runaway showed that the development of the gases took place rapidly and after the maximum temperature was reached no further

gases were released. This was also seen in the gas volume measurement in which the emitted gas volume during thermal runaway occurred in a few seconds.

Figure 33 compares the gas compositions of all investigated cyclically aged cells. All of the samples were taken during the thermal runaway.

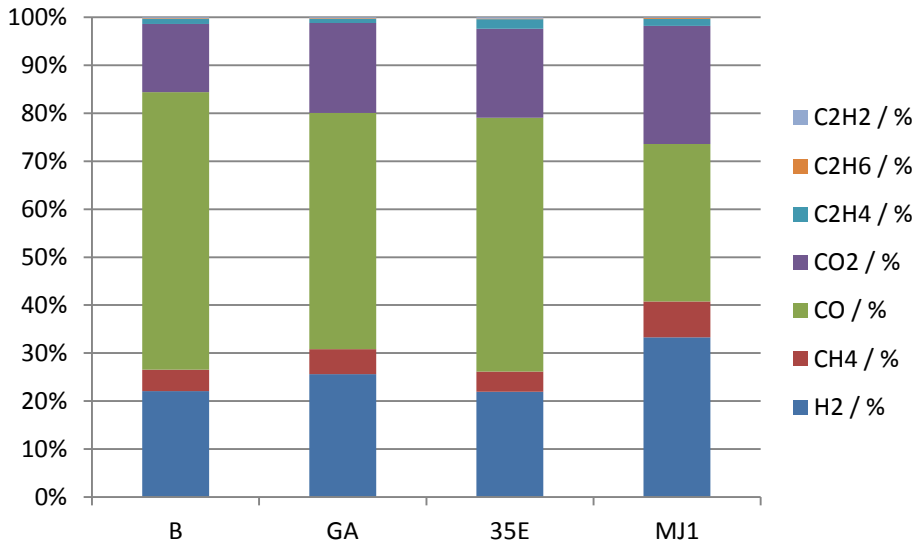

Figure 33: Gas composition of the cyclically aged cells after the thermal runaway.

The cells B, GA and 35E have very similar compositions, only the MJ1 has more H_2 and CO_2.

Figure 34 shows the gas compositions of all calendrically aged cells.

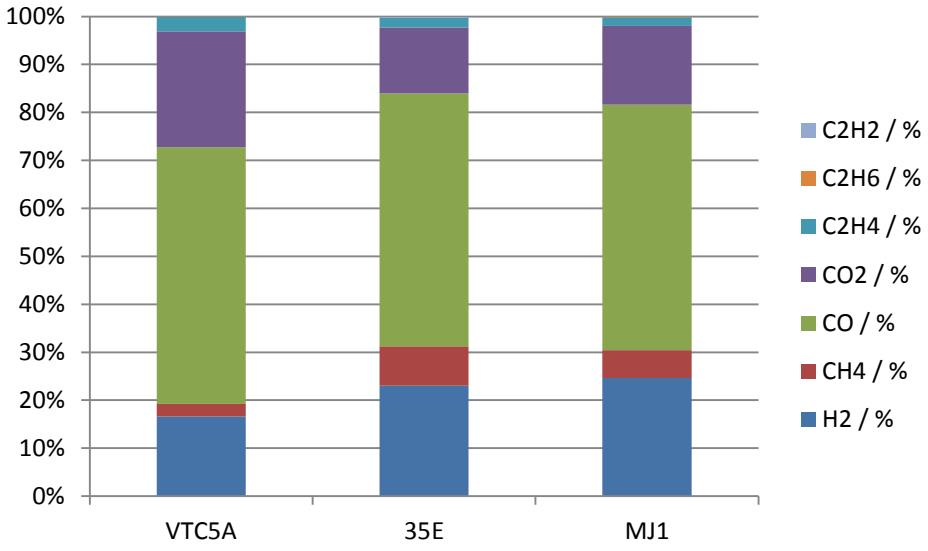

Figure 34: Gas composition of the calendrically aged cells after the thermal runaway.

The HE4 cell was not on the figure, because the cells were heated up to 700 °C to enforce the thermal runaway. No samples were taken for comparability reasons. Because all experiments were realized with the DC heating device by 70 or 140 W oven performance, only at the HE4 attempt the AC device was used. The MJ1 and 35E cell were nearly identical, though the VTC5A produced more CO_2 and lesser H_2.

Figure 35 displays the gas compositions of the new cells at a heating performance of 140 W.

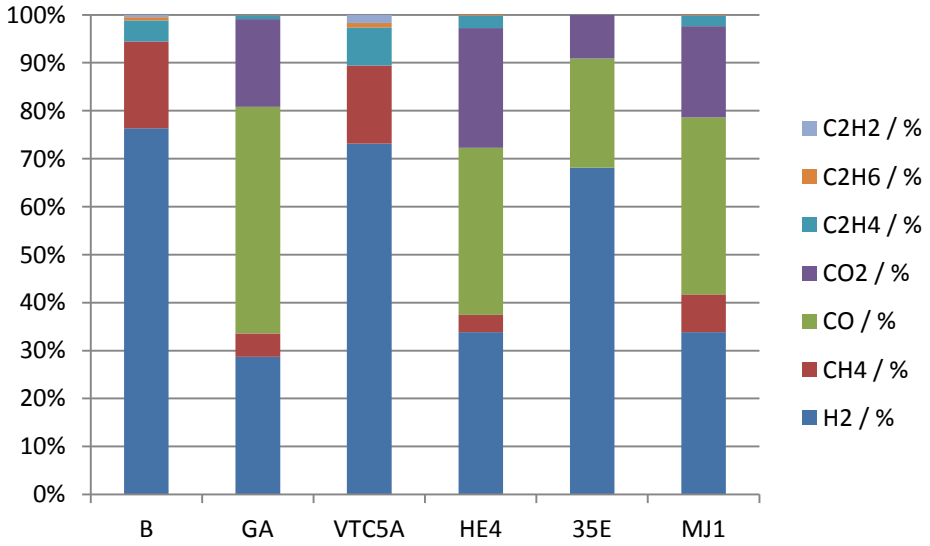

Figure 35: Gas composition of the new cells at 140 W oven performance after the thermal runaway.

The gas composition of this new cells showed high comparability of the cell types of B and VTC5A. This types produced a lot of hydrogen and carbon monoxide. In contrast the GA, HE4 and the MJ1 emitted H_2 and CO to similar parts. The CO_2 fraction indicated the progressing towards thermal runaway, the thermal runaway itself also generates other gaseous components like CO, CH_4 and H_2. The 35E is the only one, which released no methane and short-chain hydrocarbons such as C_2H_2, C_2H_4 or C_2H_6.

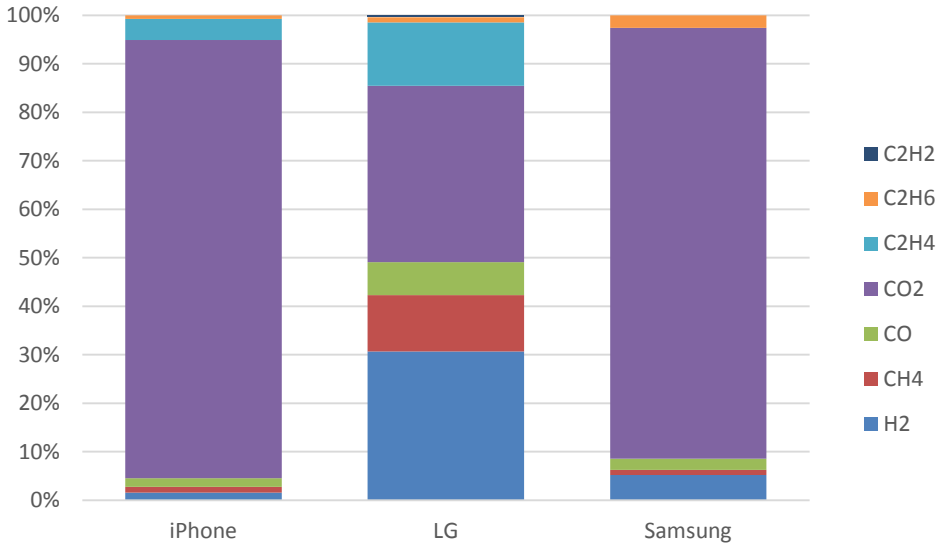

Figure 36: Gas composition of the smartphone cells.

Figure 36 shows the gas composition of the smartphone pouch cells. In experiments conducted on the Apple and Samsung cells the moment of sampling was estimated and gas was collected at equal time intervals, as no thermal runaway was occurring. For Figure 36 the fractions were selected in the exothermic phase. Compared to the LG is standing the Apple and Samsung cells which showed no thermal runaway event. At the Apple and Samsung cell was observed that the bulk of the gas composition consists of CO_2. This CO_2 comes from the plastic of the packaging in which the cell is located but also by the decomposition process in the cell itself. The $LiMO_2$ (M = metal) of the cathode is reduced when the cell is heated up. The evolved O_2 forms CO_2 in connection with the carbon anode (carbon black C), the electrolyte (for example: EC $C_3H_4O_3$) and the separation (for example: PE $(C_3H_6)_n$).

Figure 37: expanded iPhone cell after experiment with the DC heating device and 70 W oven performance

The cell expands until the packaging opens somewhere in the plastic welding around the battery (Figure 37). In this case the cell was opening at the electrodes. This meant that gas evolving chemical reactions were taking place. In addition, the short-chain hydrocarbons such as C_2H_4 and C_2H_6 and the H_2 development within the Samsung cell were signs therefore as well. Only the LG cell displayed a thermal runaway event and produced a lot of H_2, CO, CH_4 and CO_2. This shows that H_2, CO and CH_4 were mainly products of the thermal runaway.

4 CONCLUSIONS

Lithium-ion batteries have great advantages over other battery types. But the safety issue remains an obstacle in many high-tech areas such as electric vehicles and electrical storage devices. This work shows that the safety concerns with respect to lithium ion cells can not be underestimated.

The main results of this work are:

1. The scientific description of the thermal runaway is very complex and involves material science, chemistry and engineering. The material and design of the cell have a big influence on the maximum, onset and venting temperatures and on the emitted gases by thermal runaway conditions.

2. During the 1st venting event the cells develop mainly CO_2. The thermal runaway reactions produce additionally high amounts of H_2, CH_4 and CO.

3. The cathode material and the nominal capacity of the investigated cells are similar, but the results of temperature and gas compositions vary drastically.

4. New generation smartphone batteries are difficult to force into a thermal runaway event.

5. Exertion of a passive pressure, i.e. a tight fitting containment like a phone containing a cell, was not examined. This type of experiment could give additional insights into the effects of pouch cell inflation.

6. The informative value of monitoring the OCV of the cells was little.

7. The maximum temperatures during the thermal runaway varied for the various cell types as well as for the same cell type with the same test conditions

8. The exhaust gas analyses revealed the production of large volumes (over 6000 cm^3) of toxic and combustible gases such as H_2, CH_4 and CO.

In the course of this work new and also aged cells were examined. The lithium-ion batteries have a very good cycle resistance but low thermal stability. The first outgassing of the aged cells starts at lower temperatures. On the other hand T_{TR}, which

shows the beginning of the heating rate of 2 °C/min for experiments with 70 W and 4 °C/min by 140 W furnace performance, was reached at higher temperature in the case of the B, VTC5A and 35E cells. It is supposed that low reactivity due to aging leads to earlier but slower gas formation in the beginning of the thermal ramp, but the effects of the aging process also encourage a later start (T_{TR}) of thermal runaway event. The GA and MJ1 show similar results for aged and new cells. Only the calendically aged HE4 could not be forced to the thermal runaway under standard conditions with the electrical heating power for the oven of 70 W. This was only possible with a power of a stronger AC heating device. This cell is the safest of these test series.

Electrode materials, electrolytes and cell types show different thermal runaway behaviors and are crucial for the thermal stability of the battery. In order to avoid the runaway event of lithium-ion cells in accumulator packs, critical temperatures have to be avoided or new materials for safer use have to be applied.

5 LIST OF FIGURES

6 LIST OF TABLES

7 REFERENCES

[1] Intrinsic Safety and Risk of Automotive Li-Ion Batteries, Kooperative F&E-Projekte, *„Projektbeschreibung für Förderungsansuchen“*, Abwicklungsstelle Österreichische Forschungsförderungsgesellschaft mbH (FFG), Version 1.5, 2013.

[2] X. Feng, M. Fang, X. He, M. Ouyang, L. Lu, H. Wang und M. Zhang, *„Thermal runaway features of large format prismatic lithium ion battery using extended volume accelerating rate calorimetry“*, Journal of Power Sources, pp. 294-301, 2014.

[3] T. F. Stocker, D. Qin, G. K. Plattner, L. V. Alexander, S. K. Allen, N. L. Bindoff, F. M. Breon, J. A. Church, U. Cubasch, S. Emori, P. Forster, P. Friedlingstein, N. Gillett, J. M. Gregory, D. L. Hartmann, E. Jansen, B. Kirtman, R. Knutti , K. Krishna Kumar, P. Lemke, J. Marotzke, V. Masson-Delmotte, G. A. Meehl, I. I. Mokhov, S. Piao, V. Ramaswamy, D. Randall, M. Rhein, M. Rojas, C. Sabine, D. Shindell, L. D. Talley, D. G. Vaughan und S. P. Xie, *„Technical Summary in Climate Change 2013: The Physical Science Basis“*, Cambridge University Press, Cambridge, 2013.

[4] Königseder, A., 2016: *Investigation of the Thermal Runaway in Lithium Ion batteries*. Masterarbeit, Institut für Chemische Verfahrenstechnik und Umwelttechnik, Technische Universität Graz.

[5] C. Julien, Design considerations for lithium batteries, in: C. Julien, Z. Stoynov (Eds.), *Materials for Lithium-Ion Batteries*, Kluwer Academic Publishers, Netherlands, 2000, pp. 1–20.

[6] C.-Y. Jhu, Y.-W. Wang, C.-M. Shu, J.-C. Chang und J.-C. Wu, *„Thermal explosion hazards on 18650 lithium ion batteries with a VSP2 adiabatic calorimeter“*, Journal of Hazardous Materials 192, pp. 99-107, 2011.

[7] Linkedin, https://www.linkedin.com/pulse/global-market-lithium-ion-batteries-forecaststrends-chepyala, on 26.06.2017

[8] A. Dinger, R. Martin, X. Mosquet, M. Rabl, D. Rizoulls, M. Russo und G. Sticher, „*Batteries for Electric Cars*“, Boston Consulting Group, Boston, 2010.

[9] L. H. Saw, Y. Ye und A. A. Tay, *„Integration issues of lithium-ion battery into electric vehicle battery pack“,* Journal of Cleaner Production, pp. 1032-1045, 2016.

[10] D. H. Doughty und A. A. Pesaran, *„Vehicle Battery Safety Roadmap Guidance“,* National Renewable Energy Laboratory, Denver, Colorado, 2012.

[11] Q. Wang, P. Ping, X. Zhao, G. Chu, J. Sun und C. Chen, *„Thermal runaway caused fire and explosion of lithium ion battery“,* Journal of Power Sources, pp. 210-224, 2012.

[12] D. Doughty und P. E. Roth, *„A General Discussion on Li Ion Battery Safety“*, The Electrochemical Society, New Jersey, USA, 2012.

[13] M. Wakihara, *Mater. Sci. Eng. Rep. 33* (2001) 109–134

[14] V. Etacheri, R. Marom, R. Elazari, G. Salitra, D. Aurbach, *Energy Environ. Sci. 4* (2011) 3243–3262.

[15] F. Torabi, V. Esfahanian, *J. Electrochem. Soc. 158* (2011) A850–A858.

[16] R.M. Spotnitz, J. Weaver, G. Yeduvaka, D.H. Doughty, E.P. Roth, *J. Power Sources 163* (2007) 1080–1086.

[17] A. Hammami, N. Raymond, M. Armand, *Nature 424* (2003) 635–636.

[18] Q.S. Wang, P. Ping, J.H. Sun, *Nonlinear Dynam. 61* (2010) 763–772.

[19] K. Kumaresan, G. Sikha, R.E. White, *J. Electrochem. Soc. 155* (2008) A164A171.

[20] Q.S. Wang, J.H. Sun, G.Q. Chu, *“Fire Safety Science – Proceedings of the Eighth International Symposium International Association for Fire Safety Science”*, Beijing, 2005, pp. 375–382.

[21] G.H. Kim, A. Pesaran, R. Spotnitz, *J. Power Sources* 170 (2007) 476–489.

[22] R. Spotnitz, J. Franklin, *J. Power Sources* 113 (2003) 81–100.

[23] M. Lammer, A. Königseder, V. Hacker, *“Holistic methodology for characterisation of the thermally induced failure of commercially available 18650 lithium ion cells”*, Technische Universität Graz, 2017

[24] N.N. Semenov, *“Some Problems in Chemical Kinetics in Reactivity”*, Princeton University Press, New Jersey, 1959.

[25] A. W. Golubkov, S. Scheikl, R. Planteu, G. Voitic, H. Wiltsche, C. Stangl, G. Fauler, A. Thaler und V. Hacker , „*Thermal runaway of commercial 18650 Li-ion batteries with LFP and NCA cathodes - impact of state of charge and overcharge,“* Royal Society of Chemistry, pp. 57171-57186, 2015.

[26] Energy Company, SANYO Electric Co. Ltd., Lithium-Ion Battery Business Unit, Battery System Management Department, 2012, *“Specification of Lithium Ion battery (Cylindrical Typ)”*, File-No. NCR18650-068, Osaka

[27] Rechargeable Battery Business Division, SANYO Electric Co. Ltd.; T. Higami, Y. Nashimuri, M. Seki, T. Nishitani, H. Yoneda, 2015, *“Lithium Ion Battery Specification (Cylindrical Typ)”*, File-No. NCR18650-618, Osaka

[28] Taiwan Commodity Inspection Act, 2014, *“Lithium-Ion Rechargeable Battery”*, IEC62133 2nd, File No. UL1642; US18650VTC5A, Taiwan

[29] LG Twin Tower 128; K. Hyoungkwon, 2013, *“Lithium Ion LG 18650 HE4 2500mAh”*, Document-No. BCY-PS-HE4-Rev0, Seoul

[30] Samsung SDI Co. Ltd., Cell Business Division; K. Yunwoong , 2015, *“Specification of Product for Lithium-ion rechargeable cell”*, Spec-No. INR18650-35E; Version No. Ver. 1.1, Kyunggi-do

[31] LG Chem; K. Dong Myung, 2014, *“Product Specification Rechargeable Lithium Ion Battery INR18650 MJ1 3500mAh”*, Doc.-No. LRB-PS-CY3450_MJ1, Seoul

[32] C. J. Orendorff, J. Lamb, L. A. M. Steele, S. W. Spangler und J. Langendorf, *„Quantification of Lithium-ion Cell Thermal Runaway Energetics“,* Sandia National Laboratories, Albuquerque, 2016.